Vol. 10 No.1 March 2022 ISSN 2321-0214

DISCOURSE

Xaverian Research Journal

Peer Refereed Bi-annual
Interdisciplinary Studies and Research

Researh Promotion Council
St.Xavier's College for Women Aluva
Aluva P.O., Ernakulam Dist., Kerala
Website : www.stxaviersaluva.ac.in

DISCOURSE

Xaverian Research Journal

Vol. 10 No.1 March 2022

ISSN 2321-0214

Peer Refereed Bi-annual Interdisciplinary Studies and Research

(Published in March & September)

Published by

Research Promotion Council

St. Xavier's College for Women, Aluva

Nationally Re-accredited with A Grade

Website: http://www.stxaviersaluva.ac.in

E-mail:discourse2013@gmail.com

Tel:0484-2623240, Fax: 0484-2628840

Discourse is a peer refereed biannual interdisciplinary journal published by St. Xavier's College for Women, Aluva. It was started in the year 2013 with the aim of disseminating information in the field of science and humanities to the members of academic community. Contributions in the form of research articles, review articles and short communications are welcome.

The vision of the College is to uplift the educational, social, cultural and vocational status of women by empowering them with academic excellence, personality development and spiritual enlightenment.

Discourse invites all academicians/researchers to place order for the journal by paying an amount of Rs.1000/- per volume (Two issues each in March and September) either by cash or cheque in favour of the Principal, St. Xavier's College for Women, Aluva along with the filled in order form to the following address:
The Chief Editor,
Discourse,
St. Xavier's College for Women,
Aluva, Ernakulam Dist., Kerala
Pin 683101
Email: discourse2013@gmail.com
Please provide the manuscripts one month prior to the month of publication (February and August)

Contents

Research Articles

STRUCTURAL AND MAGNETIC CHARACTERIZATION OF COPPER SUBSTITUTED COBALT MAGNESIUM MIXED FERRITE NANOPARTICLES

Ansalna M.R., Siya Tresa Jiji, Tharneem V.A., Dhanya Jose and Sheena Xavier

Department of Physics, St. Xavier's College for Women, Aluva
***Corresponding Author email id:** sheenaxavier@stxaviersaluva.ac.in

Abstract

The present research work is focused on the structural and magnetic characterization of copper substituted cobalt magnesium mixed ferrite (CMCF) nanoparticles. The powder samples of $Co_{0.5}Mg_{0.5-x}Cu_xFe_2O_4$ (x=0.0, 0.01, 0.02, 0.03) ferrites were prepared by sol-gel synthesis and were sintered at 400^oC for two hours. The samples were labelled CMCF0, CMCF1, CMCF2 & CMCF3. The structural and magnetic properties of the mixed ferrite were studied. The phase identification, lattice parameter and hence the crystalline size determination were carried out by using X-ray diffraction and revealed that all particles exhibited single phase cubic spinel structure. The size of the nanocrystalline ferrites remains within the range 12-18nm. The FTIR spectra exhibited two intense bands in the range 580cm^{-1} to 575cm^{-1} and 425cm^{-1} to 428cm^{-1}. FTIR spectral analysis confirmed the spinel structure. The Transmission Electron Microscopy (TEM) image of CMCF0 was obtained and analysed. EDAX analysis was done on CMCF0 and its compositional purity was established. The magnetic properties have been studied using Vibrating Sample Magnetometer (VSM). The saturation magnetization, coercivity and remanent magnetization were calculated from the M-H loops. CMCF samples exhibit hysteresis loops of ferrimegnetic behaviour. They have high coercivity and moderate saturation magnetization.

Keywords: Cobalt magnesium mixed nanoferrite, Sol-Gel synthesis, Characterisation

Introduction

The application of nanomaterials in the biomedical field allows solving many issues such as targeted drug delivery (Arruebo *et al.*, 2008), contrast-enhancing dye in magnetic resonance imaging (MRI) (Ahmad *et al.*, 2015), mediators for hyperthermia applications (Jordan *et al.*, 1993) cell labelling and tracking (Knollmann *et al.*, 1998), angiography with MRI (Plank *et al.*, 2009), cellular transfection using magnetic fields (Mandeville *et al.*, 1998), cerebral blood volume experiments of functional MRI (fMRI) (Maritim *et al.*, 2017), drug distribution in the brain (Lopez-Abarrategui *et al.*, 2016) and antimicrobial activity agent. Surface functionalized spinel ferrite nanoparticles such as $MnFe_2O_4$, $MgFe_2O_4$, $CoFe_2O_4$, $ZnFe_2O_4$ and Fe_3O_4 are excellent mediators for cancer thermotherapy and MRI contrast agents (Albino *et al.*, 2009). These nanoparticles are biocompatible, biodegradable, possess high transition temperatures, and have excellent chemical stability. Moreover, nano-magnetism of ferrite nanoparticles provides the opportunity for several biomedical applications because these possess higher magnetic susceptibility than normal superparamagnetic materials and negligible coercivity and retentivity.

Properties of ferrites depend on their composition and microstructure, which in turn depend on their synthesis processes. There are various chemical and physical methods (Amighian *et al.*, 2006) to synthesize ferrite nanoparticles, such as chemical co-precipitation, sol-gel auto combustion, reverse micelle, microwave hydrothermal, sonochemical, forced hydrolysis, one-step, high energy ball milling, solvothermal, and microemulsion method. The sol-gel technique is probably most effective method for the synthesis of homogeneous nano-sized particles. This process offers the possibility of a generalized approach to the production of both single and complex oxide nanoparticles. This technique involves hydrolysis and condensation reactions of metal precursors, such as salts

or alkoxides, leading to the formation of three-dimensional inorganic networks. Due to good stoichiometric control and production of ultrafine particles in nano-range at relatively low temperatures, sol-gel technique is an attractive method for the preparation of nano-ferrites (Jacob *et al.*, 2011). This method is employed to obtain improved powder characteristics, more homogeneity, narrow particle size, thereby influencing structural, electrical and magnetic properties of spinel ferrites.

Further, the proper analysis of properties using various characterization techniques can lead to the design of nanomaterials for different applications. Hence the prepared materials were analysed using various analytical instruments. Characterization techniques include X-ray Diffractometer (XRD), Fourier transform infrared spectroscopy, Energy-dispersive X-ray spectroscopy and Vibrating Sample Magnetometer.

Cobalt ferrite ($CoFe_2O_4$) belongs to the family of AB_2O_4-type inverse spinel ferrites and has been studied extensively because of its interesting magnetic properties. From the crystallography viewpoint, in the Cobalt ferrites, A sites are occupied by Fe^{3+} ions, while B sites are equally populated by Co^{2+} and Fe^{3+} ions. Cobalt ferrite can be represented as $(Co_xFe_{1-x})[Co_{1-x}Fe_{1+x}]O_4$ where x depends on thermal treatment and preparation conditions. Since the FeA^{3+} - FeB^{3+} super-exchange interaction is normally different from the CoA^{3+}-FeB^{3+} interaction, the variation of the cation distribution over A and B sites in the spinel depend on the bond length and leads to the different magnetic properties of these oxides, even though the chemical composition of the compound remains the same. The inter-ionic distances can also vary as a function of synthesis method. This variation affects the magnetic properties like saturation magnetization and Curie point. The saturation magnetization is a result of the sum of unpaired spins of cations. Cobalt ferrite has special physical and

mechanical properties which lead to its wide application in nanomedicine. It is a hard magnetic material with high Curie temperature T_C, high coercivity at room temperature, high saturation magnetization at room temperature, high anisotropy constant and high magnetostriction. Furthermore, it shows excellent chemical stability, mechanical hardness, wear resistance, ease of synthesis and electrical insulation. The above-mentioned properties make cobalt ferrite one of the most promising candidates for medical applications, including magnetic drug-delivery, radiofrequency hyperthermia, magnetic resonance imaging (MRI) and medical diagnostics (Thankachan *et al.,* 2013). Cobalt ferrite nanoparticles also find application in high-frequency magnets, magnetic bulk cores, magnetic data-storage devices, microwave absorbers etc.

Materials and Methods

(a) Sample preparation

In order to prepare copper substituted cobalt magnesium mixed ferrite nanoparticles, analytical reagent (AR) grade cobalt nitrate, magnesium nitrate, copper nitrate and ferric nitrate were used as chemical precursors. Metal nitrates in the required stoichiometric ratio were dissolved in minimum amount of ethylene glycol at room temperature and the sol was heated at 60^{o}C, to obtain a wet gel. Further heating of the gel at higher temperatures led to the self-ignition. The obtained dry powder is ground well using agate mortar to form ultrafine particles of cobalt ferrite.

For the preparation of samples, metal nitrates were mixed in the appropriate stoichiometric ratio. Primarily, $Co_{0.5}Mg_{0.5}Fe_2O_4$ sample was prepared in which the ratio of Ferric nitrate to Cobalt nitrate and Magnesium nitrate was 2:1. Then, copper was doped into cobalt magnesium ferrite to obtain the mixed ferrites. The samples of $Co_{0.5}Mg_{0.5-x}Cu_xFe_2O_4$ (x=0.0, 0.01, 0.02, 0.03) ferrites were prepared in a similar manner and were sintered at 400^{o}C for two hours.

(b) Structural characterization

The structural properties of the samples were analysed using X-Ray Diffraction technique. XRD pattern analysis is used to identify crystalline phases and orientation and to determine structural properties like lattice parameter, strain, grain size, phase composition, and to measure d-spacing. By comparing the data with the known standards in the ICDD file, we can identify the structure of the unknown sample. From the 2θ values of the peaks, the lattice spacing (d) values are calculated using;

$$2dsin\theta=n\lambda$$

The lattice parameter 'a' was then computed using;

$$d_{hkl} = a \Big/ \sqrt{(h^2 + k^2 + l^2)}$$

crystallite size is calculated from the Full Width at Half Maximum (*FWHM*) of a diffraction peak by Scherrer formula,

$$D = K\lambda \Big/ \beta cos\theta$$

where D is the crystallite size, K is the shape factor ($K \approx 1$), λ is the wavelength of radiation, β is the angular width in radians.

The X-ray density was calculated using;

$$\rho_x = \frac{8M}{Na^3}$$

where M is the molecular weight (gm) of the sample, N is Avogadro's number and 'a' is the lattice parameter(Å) (Kittel and McEuen, 2018).

Fourier transform infrared spectroscopy can be used to detect changes in coordination and configuration of molecular species in a system. In an infrared spectrum, the absorption or transmittance peaks correspond to the frequencies of vibrations between the bonds of the atoms making up the material. From the characteristic peaks, different functional groups present in the compound can be identified. IR spectra of the investigated nano ferrite samples were recorded using FTIR spectrometer in the wave number range 4000 to 400 cm^{-1} (Cullum and Vo-Dinh, 2003).

TEM is a powerful imaging tool with high resolution to analyse the microstructure. If the resolution of the microscope is sufficiently high and a suitable crystalline sample oriented along a zone axis, then high resolution TEM images can be obtained. In a TEM the electron beam is focused on to the sample. The high magnification or resolution of TEM is given by

$$L = \frac{h}{\sqrt{(2mqV)}}$$

where m and q are the electron mass and charge, h the Planck's constant and V is the potential difference through which the electrons are accelerated (Smith, 2018).

Energy-dispersive X-ray spectroscopy is an analytical technique used for the elemental analysis or chemical characterization of a sample. EDS can be used to determine which chemical elements are present in a sample, and can be used to estimate their relative abundance. EDS also helps to measure multi-layer coating thickness of metallic coatings and analysis of various alloys. The chemical information can be visualised as elemental mapping and line scans. In this way, X-rays can be used to identify each element that exists in a sample (Watt, 1997; www.thermofisher.com).

Vibrating Sample Magnetometer is a versatile technique for measuring the magnetic moment of a sample when it is vibrated perpendicularly to a uniform magnetizing field. The VSM technique can be used to obtain the magnetic moment information of samples based on Faraday's law of magnetic induction. The hysteresis loop of the samples can be studied using VSM. The magnetic properties of the samples such as saturation magnetization (M_s), coercive field (H_c), remanence and remanent ratio can be obtained from the analysis of hysteresis loop (Krishnan and Banerjee, 1999; Denardin *et al*., 2002).

Results

XRD Analysis

XRD analysis is a useful way to get the structural information of a material. To study the structural characteristics of copper substituted cobalt magnesium ferrite nanoparticles, AXS D8 Advance diffractometer was used. In this case, X-ray diffractometer is equipped with Cu-Kα radiation of wavelength 1.5406Å in the range of 2θ= 20^o to 80^o.

(a) Phase Analysis

The structural view of CMCF samples were confirmed from XRD analysis. Figure 1 shows the X-Ray diffraction patterns of the CMCF mixed ferrites. The XRD patterns show 5 sharp peaks and the peaks can be indexed as (220), (311), (400), (422), (511) and (440). All the peaks correspond to the standard diffraction peaks of spinel ferrites and are in exact agreement with the data provided by the ICDD. XRD data indicate that the synthesized samples crystallize in the spinel phase. Here the calculations for the prominent peaks (311) and (440) are carried out. The position of the X-ray peaks and their corresponding miller indices are given in table 1.

Table 1. Position of the X-ray peaks and corresponding miller indices

Samples	Miller indices (hkl) of the X-ray peaks and their position in 2θ degrees	
	(311)	(440)
CMCF0	35.300	62.528
CMCF1	35.319	62.565
CMCF2	35.293	62.527
CMCF3	35.369	62.526

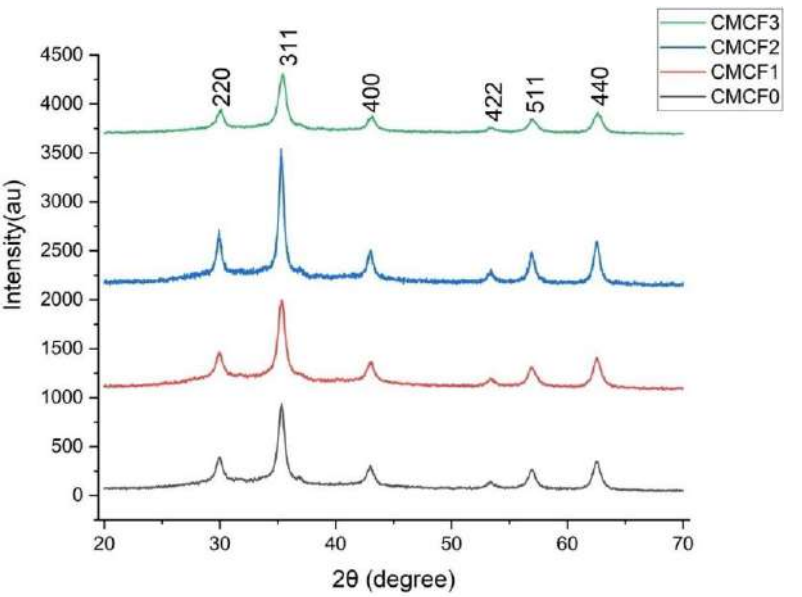

Figure 1. XRD patterns of CMCF samples

(b) Analysis of Structural Parameters

Using the XRD data, the lattice constant (a) for the prominent peaks of each sample is calculated from the knowledge of the interplanar spacing (d), and the miller indices (hkl). The crystallite size (D) is calculated using the Scherrer formula. The X-ray density (ρ_X) is determined from the calculated values of the lattice constant (Table 2). The XRD pattern show a single-phase structure for all the samples and all the different peaks (220), (311), (400), (422), (511) and (440) can be indexed to the cubic spinel structure.

Table 2. Comparison of structural parameters of samples

Sample	D(nm)	*a*(Å)	ρ(gm/cm^3)
CMCF0	13.699	8.411	4.851
CMCF1	13.320	8.406	4.868
CMCF2	17.939	8.412	4.862
CMCF3	12.711	8.397	4.901

The crystallite size (D) of the nanocrystalline ferrites remains within the range 12-18nm for the studied compositions which can be attributed to the decrease of Mg having higher lattice constant. The variation in lattice parameter does not show a linear increase or decrease. The lattice constant ranges from 8.397Å to 8.411 by Cu^{2+} substitution which is attributed to the simultaneous change in ratios of Cu^{2+} and Mg^{2+} ions. The X-ray density (ρ) was calculated using the following equation:

$$\rho_x = \frac{8M}{Na^3}$$

Here ρ is inversely proportional to cube of lattice parameter a. When the result is analysed, we see that, as the lattice parameter decreases, there is a corresponding increase in X-ray density.

FTIR Spectral Analysis

Infrared spectra of the investigated nano ferrite samples were recorded using FTIR spectrometer. FTIR spectra were recorded for the dried samples of ferrites using Thermo Nicolet, Avatar 370 spectrometer. From the characteristic absorption bands, different functional groups present in the composite can be identified. Hence IR spectroscopy is very useful in material characterization. Figure 2 shows the FTIR spectra of the studied samples.

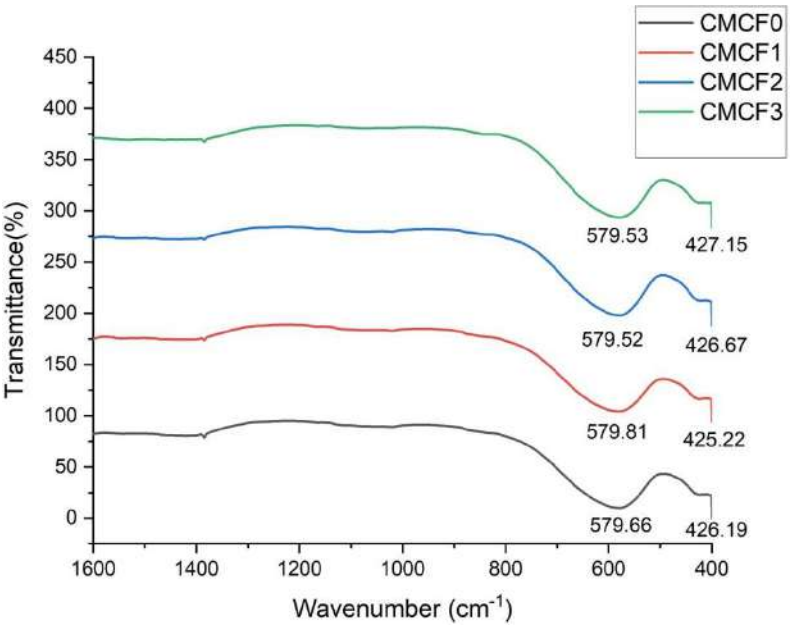

Figure 2. FTIR spectra of CMCF samples

The spectra of CMCF samples exhibit two intense bands in the range, 580cm^{-1} to 575cm^{-1} and 425cm^{-1} to 428cm^{-1} belonging to the stretching vibration modes associated to the metal-oxygen absorption bands in the crystalline lattice of Cu substituted cobalt magnesium ferrites. They are characteristically pronounced for all spinel structures and for ferrites in particular. The occurrence of these bands at 580cm^{-1} to 575cm^{-1} and 425cm^{-1} to 428cm^{-1} are assigned to tetrahedral and octahedral complexes respectively. The difference in band positions is attributed to the difference in Fe^{3+} to O^{2-} distances for the tetrahedral and octahedral complexes. In summary, FTIR absorption spectroscopy confirms the XRD structural characterization.

Transmission Electron Microscopy (TEM) Analysis

The Transmission Electron microscope image of CMCF0 sample is shown in figure 3. The TEM image was obtained using TEM Philips CM 200. The size of more than 200 nanoparticles is determined from different images of the same

sample using Image J software and size distribution histogram is drawn as given in figure 4. Most of the nanoparticles are almost spherical in shape. However, a slight agglomeration is noticed. It can be seen that the particles have narrow size distribution. From the size distribution histogram, the most probable diameter of the particles is determined to be 13.77 nm. The size of the CMCF ferrite nanoparticles obtained by TEM is in good agreement with the crystalline size calculated from X-ray diffraction pattern using Scherrer formula.

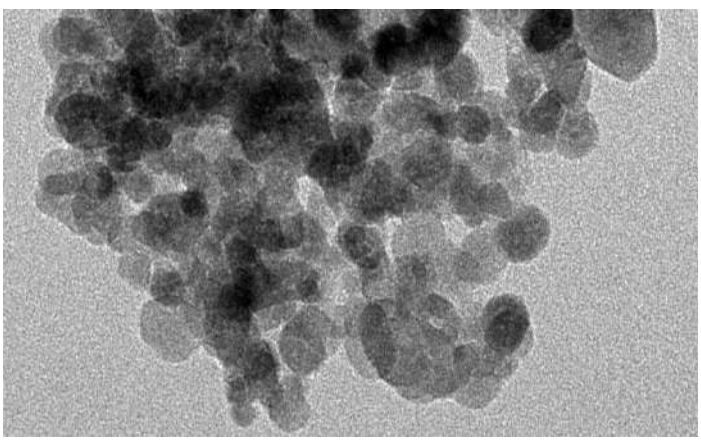

Figure 3. TEM image of CMCF0

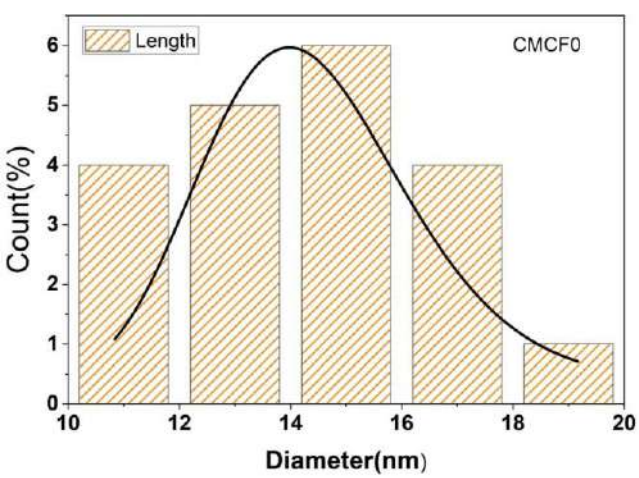

Figure 4. Size distribution histogram of CMCF0

EDAX Analysis

The energy dispersive X-ray spectrum of sample CMCF0 is analysed using Jeol 6390LV Scanning Electron Microscope at accelerating voltage of 0.5kV to 30kV. The EDS/EDAX spectrum of CMCF0 obtained is given in figure 5. The Dispersive Energy (KeV)-Counts curve of the sample shows that each element has a unique atomic structure, allowing a unique set of peaks on its X-ray emission spectrum. The elements present are O, Fe, Mg and Co. It can be seen that Fe is the dominant element in the sample.

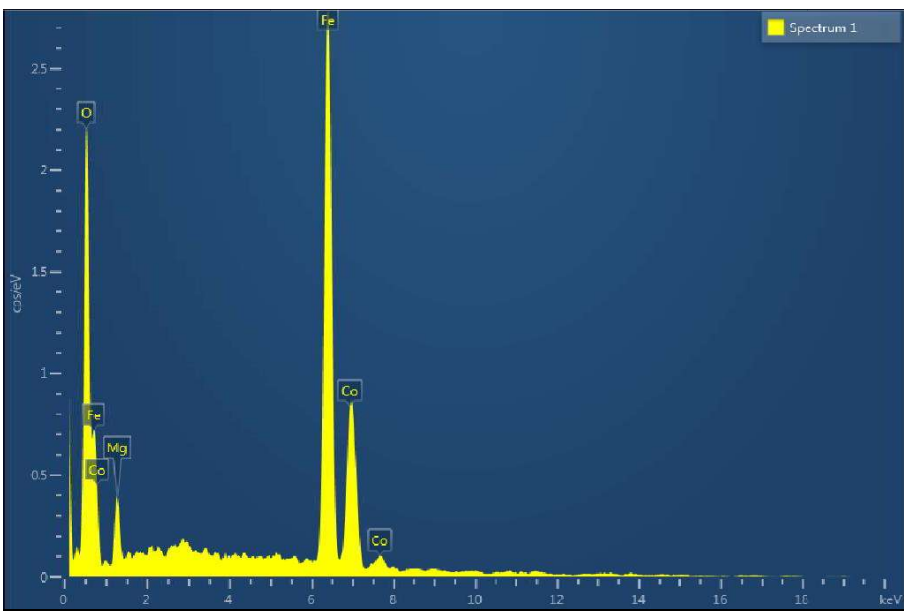

Figure 5. EDS spectrum of CMCF0

The EDS Analysis results in table 3 gives an overview of the elements present in CMCF0 and their corresponding weight and atomic percent. The elements belong to the K series. That is the electron moves towards the vacancy in K shell created by the displaced electron (www.thermofischer.com). No trace of impurity is found. This means that the compositional stoichiometry of the ferrite powders exists right till their nanosized structure state.

Table 3. EDS Analysis results of CMCF0

Element	Line Type	Weight %	Atomic %
O	K series	21.58	47.5
Mg	K series	4.42	6.40
Fe	K series	56.88	35.87
Co	K series	17.11	10.23
Total		100	100

Vibrating Sample Magnetometer (VSM) Analysis

The magnetic properties are investigated with a vibrating sample magnetometer (Lakeshore VSM 7410) at room temperature. The figure 6 show the field dependent magnetization (M-H) curves for the samples at room temperature under an applied field of 15 kOe. The hysteresis loops of the ferrite system are given in stacked form. The values of hysteresis measurement of coercive field (H_c), saturation magnetization (M_s) and remanent magnetization (M_r) of the samples are tabulated.

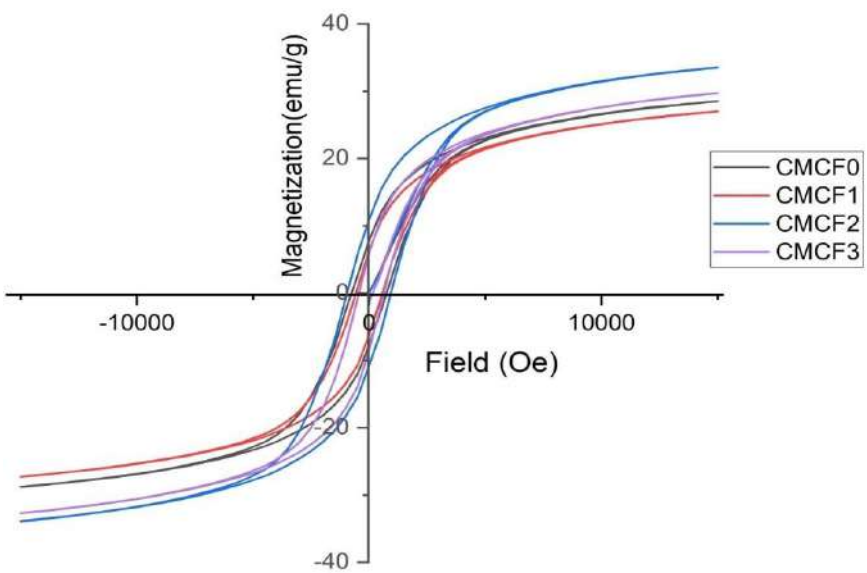

Figure 6. Hysteresis loops of CMCF samples

The magnetic properties for all the samples are summarized in Table 3.4. CMCF sample exhibit hysteresis loops of typical magnetic behaviour, indicating the presence of ordered magnetic structure in the spinel system. They have high coercivity (H_C) and moderate saturation magnetization (M_s).

The magnetic behaviour of ferrite nanoparticles depends on the method of synthesis, cation distribution between octahedral and tetrahedral site and the crystalline size (Hsiang and Wu, 2015). There is a nonlinear variation of magnetic parameters. The saturation magnetisation ranges from 25.286 to 32.192 emu/g while the coercivity lies in the range 540.24 to 939.33 Oe. The remanent ratio (M_r/M_s) of the samples lies in the range 0.2 to 0.32 and the retentivity in the range 7 to 8 emu/g. The lowest value of coercivity and remanent ratio is shown by CMCF3 sample (table 4).

Table 4. Saturation Magnetization, Coercivity, Retentivity and Remnant ratio of the samples

Sample	Saturation Magnetization (M_s) (emu/g)	Coercivity (H_C) (Oe)	Retentivity (M_r) (emu/g)	Remnant ratio (M_r/M_s)
CMCF0	28.665	754.90	7.788	0.2717
CMCF1	27.141	570.33	6.304	0.2322
CMCF2	25.286	939.33	8.107	0.3206
CMCF3	32.192	540.24	7.430	0.2307

Conclusions

The sol gel process being one of the most effective methods for the synthesis of homogeneous nano-sized particles was used for the synthesis of the copper substituted cobalt magnesium ferrite $Cu_xMg_{0.5-x}Co_{0.5}Fe_2O_4$ (x=0.0, 0.01, 0.02, 0.03) nanoparticles. Powdered samples were used for the XRD, FTIR, VSM

& EDAX analyses. The particle size of CMCF was calculated using the TEM image. These analyses revealed the following results:

1) The XRD patterns of the four samples (CMCF0, CMCF1, CMCF2 and CMCF3) confirmed the cubic spinel structure. The crystallite size (D) of the nanocrystalline ferrites remains within the range 12-18nm for the studied compositions. The value of lattice parameter is high in the case of CMCF0 which then decreases on the addition of copper. The variation in lattice parameter does not show a linear increase or decrease. This may be due to the simultaneous change in ratios of Cu^{2+} and Mg^{2+}.
2) The FTIR spectra exhibit two intense bands in the range $580cm^{-1}$ to $575cm^{-1}$ and $425cm^{-1}$ to $428cm^{-1}$ belonging to the stretching vibration modes associated to the metal-oxygen absorption bands in the crystalline lattice of Mg and Cu substituted cobalt ferrites. FTIR absorption spectroscopy identified the spinel structure and confirmed the XRD structural characterization.
3) From the EDAX spectrum of CMCF0, it can be seen that Fe is the dominant element followed by Oxygen, Cobalt and Magnesium. All elements belong to the K series. Thus, the electron moves towards the vacancy in K shell created by the displaced electron. Also, no trace of impurity is found.
4) From the TEM image of CMCF0, it can be seen that most of the nanoparticles are almost spherical in shape. However, a slight agglomeration is noticed. It can be seen that the particles have narrow sized distribution. The most probable diameter of the particles is determined to be 13.77nm which is in good agreement with the crystalline size calculated using Scherrer formula.

5) The magnetic properties were investigated using VSM. CMCF sample exhibit hysteresis loops of typical magnetic behaviour, indicating the presence of ordered magnetic structure in the spinel system. They have high coercivity and moderate saturation magnetization. CMCF0 is found to have high saturation magnetisation. The remanent ratio of the samples lies in the range 0.2 to 0.32.

Acknowledgement

The authors would like to acknowledge the Science Education Division, Kerala State Council for Science Technology and Environment for their highly appreciated economic support and encouragements to pursue research career. The authors are grateful to SAIF, CUSAT and SAIF, IIT Madras, SAIF, IIT Bombay for providing the technical amenities for this research.

References

Ahmad, T., Bae, H., Iqbal, Y., Rhee, I., Hong, S., Chang, Y., ... and Sohn, D (2015) Chitosan-coated nickel-ferrite nanoparticles as contrast agents in magnetic resonance imaging. *Journal of Magnetism and Magnetic Materials*. 381: 151-157.

Albino, M., Fantechi, E., Innocenti, C., López-Ortega, A., Bonanni, V., Campo, G., ... and Sangregorio, C (2019) Role of Zn2+ substitution on the magnetic, hyperthermic, and relaxometric properties of cobalt ferrite nanoparticles. *The Journal of Physical Chemistry C*. 123(10): 6148-6157.

Amighian, J., Mozaffari, M., and Nasr, B (2006) Preparation of nano-sized manganese ferrite (MnFe2O4) via coprecipitation method. *Physica Status Solidi C.* 3(9): 3188-3192.

Arruebo, M., Fernández-Pacheco, R., Ibarra, M. R. and Santamaría, J (2007) Magnetic nanoparticles for drug delivery. *Nano today*. *2*(3): 22-32.

Cullum, B. M and Vo-Dinh, T (2003) Sample collection and preparation of liquid and solids. *Handbook of Spectroscopy*. 2: 1.

Denardin, J. C., Brandl, A. L., Knobel, M., Panissod, P., Pakhomov, A. B., Liu, H., and Zhang, X. X. (2002) Thermoremanence and zero-field-cooled/field-cooled magnetization study of Co x (SiO 2) 1− x granular films. *Physical Review B*. 65(6): 064422.

https://www.thermofisher.com/blog/microscopy/edx-analysis-with-sem-howdoes-it-work

Jacob, B. P., Thankachan, S., Xavier, S. and Mohammed, E. M. (2011) Effect of Gd3+ doping on the structural and magnetic properties of nanocrystalline Ni–Cd mixed ferrite. *Physica Scripta*. 84(4): 045702.

Jordan, A., Wust, P., Fähling, H., John, W., Hinz, A and Felix, R (1993) Inductive heating of ferrimagnetic particles and magnetic fluids: physical evaluation of their potential for hyperthermia. *International journal of hyperthermia. 9*(1): 51-68.

Kittel, C and McEuen, P (2018) *Introduction to solid state physics*. John Wiley & Sons.

Knollmann, F. D., Böck, J. C., Rautenberg, K., Beier, J., Ebert, W and Felix, R (1998) Differences in Predominant Enhancement Mechanisms of Superparamagnetic Iron Oxide and Ultrasmall Superparamagnetic Iron Oxide for Contrast-Enhanced Portal Magnetic Resonance Angiography: Preliminary Results of an Animal Study. *Investigative radiology*. *33*(9): 637-643.

Krishnan, R. V and Banerjee, A (1999) Harmonic detection of multipole moments and absolute calibration in a simple, low-cost vibrating sample magnetometer. *Review of scientific instruments*. 70(1): 85-91.

Lopez-Abarrategui, C., Figueroa-Espi, V., Lugo-Alvarez, M. B., Pereira, C. D., Garay, H., Barbosa, J. A., ... and Otero-Gonzalez, A. J (2016) The intrinsic antimicrobial activity of citric acid-coated manganese ferrite nanoparticles is enhanced after conjugation with the antifungal peptide Cm-p5. *International Journal of Nanomedicine.* 11: 3849.

Mandeville, J. B., Marota, J. J., Kosofsky, B. E., Keltner, J. R., Weissleder, R., Rosen, B. R and Weisskoff, R. M (1998) Dynamic functional imaging of relative cerebral blood volume during rat forepaw stimulation. *Magnetic resonance in medicine.* 39(4): 615-624.

Maritim, S., Coman, D., Huang, Y., Rao, J. U., Walsh, J. J and Hyder, F (2017) Mapping extracellular pH of gliomas in presence of superparamagnetic nanoparticles: towards imaging the distribution of drug-containing nanoparticles and their curative effect on the tumor microenvironment. *Contrast media and molecular imaging.*

Plank, C., Zelphati, O and Mykhaylyk, O (2011) Magnetically enhanced nucleic acid delivery. Ten years of magnetofection—Progress and prospects. *Advanced drug delivery reviews.* 63(14-15): 1300-1331.

Smith, B. (2018) *Infrared spectral interpretation: a systematic approach*. CRC press.

Thankachan, S., Jacob, B. P., Xavier, S., & Mohammed, E. M. (2013). Effect of samarium substitution on structural and magnetic properties of magnesium ferrite nanoparticles. *Journal of magnetism and magnetic materials*. 348*:* 140-145.

Watt, I. M. (1997) *The principles and practice of electron microscopy*. Cambridge University Press.

Hsiang, H. I. and Wu, J. L (2015) Copper-rich phase segregation effects on the magnetic properties and DC-bias-superposition characteristic of NiCuZn ferrites. *Journal of Magnetism and Magnetic Materials*. 374: 367-371.

TEM ANALYSIS OF LYSOGENIC VIBRIOPHAGES ISOLATED BY MITOMYCIN C INDUCTION OF ENVIRONMENTAL VIBRIOS

Linda Louis[1], Jeena Augustine[2] and Sarita G Bhat[2]

[1] Department of Zoology, St. Xavier's College for Women, Aluva, Kerala.
[2]Cochin University of Science and Technology, Kochi, Kerala
***Corresponding Author email id:** lindalouis@stxaviersaluva.ac.in

Abstract

The southern Indian state of Kerala is endemic to Cholera. Bacteriophages, whose hosts are bacterial cells, act as agents of 'mobile DNA'. The temperate bacteriophages of *V. cholerae* are the most promising candidates for the conversion of avirulent strains to virulent ones. It is important to understand the mechanisms and evolution of virulence in *V. cholerae* and of bacterial pathogenesis. Lysogenic phage induction using mitomycin C, is effective for induction of lysogenic vibrios. Differential induction and purification of vibriophages and its physicochemical characterization is an essential requirement as evidence for horizontal gene transfer by transduction. Bacteriophages encompass many types of virion morphologies and nucleic acid compositions and the six basic morphological types are exemplified by phages T4, λ, T7, φX174, MS2 and fd. Transmission Electron Microscopy based morphological analysis of phages is highly significant as it is the basis for classification of bacteriophages. Inducible prophages were detected in environmental isolates of *V. cholerae* which adds to the role of such phages in altering the pathogenic potential of host vibrio.

Keywords: Cholera, bacteriophage, vibriophages

Introduction

Marine aquaculture settings and mangrove environments of Kerala serve as reservoirs for *V. cholerae* in Kerala (Geeta and Krishnakumar, 2005). There are reports that in Kerala, most cholera outbreaks are caused by *V. cholerae* O1 El Tor belonging to Ogawa serotype (Thomas *et al*., 2008). Bacteriophages contribute significantly to the marine microbial loop and nutrient cycling in the oceans, besides serving as agents of gene transfer in the marine environment (Fuhrman, 1999). Pathogenic strains of *Vibrio cholerae* also owe much of their pathogenicity to phage conversion, with cholera toxin encoded by the temperate and filamentous phage CTXΦ (Waldor and Mekalanos, 1996). Extrinsic factors, such as large-scale weather cycles (Colwell, 1996), and intrinsic factors like the induction of bacteriophages infecting Vibrios (also called vibriophages) were shown to correlate in time with components of the epidemic cycle (Faruque *et al.,* 2000).

The serogroup O139 has evolved as a result of horizontal transfer of genes from a non-O1 strain to the seventh pandemic clone of V. cholerae O1 (Bik *et al.*, 1995; Waldor and Mekalanos, 1994). The transducing phages of *V. cholerae* are involved in the emergence of pandemic strains through biotype transition (Ogg *et al.,* 1981). Filamentous phages play critical roles in horizontal gene transfer among *V. cholerae* (Jiang and Paul, 1998; Davis and Waldor, 2003). Bacteriophages being natural viral pathogens of bacteria co-exist with their hosts, sharing the same ecological niches (Goyal *et al.*, 1987). CTXΦ, a lysogenic filamentous bacteriophage encodes *ctxAB* genes producing cholera toxin (CT) (Waldor and Mekalanos, 1996)

The discovery of a number of temperate vibriophages (Kar *et al*., 1996) is an emerging force in the appearance of the novel pathogenic clones of *V. cholerae.*

Bacteriophages were classified merely based on host specificity (Ackermann, 2007). The advent of electron microscopy enabled scientists to classify phages based on their morphology. International Committee on Taxonomy of Viruses (ICTV) is derived from the scheme proposed by Bradley (1967) using gross morphology and nature of their nucleic acid.

Currently it includes one order, 17 families and three "floating" groups (Ackermann, 2007, 2009). The large majority are double stranded DNA (dsDNA) tailed phages (Caudovirales) (Ackermann, 2007).

Materials and Methods

Vibrio cholerae isolated from water and sediment samples from aquafarms and mangroves along the coastal regions of Ernakulam and Alappuzha, Kerala, South India were screened for the presence of temperate phages. Thiosulphate Citrate Bile salt Sucrose (TCBS) agar (HiMedia, Mumbai, India) supplemented with 1% NaCl is used as selective medium for isolation of vibrios. The presumptive *Vibrio* isolates were subjected to molecular characterization using 16S rRNA partial gene sequencing with universal primer and the sequences were analysed using bioinformatic tools to identify *Vibrio cholerae* (Shivaji *et al*., 2000). These isolates, along with cultures available in Microbial Genetics Laboratory, Department of Biotechnology, Cochin University of Science and Technology were used as host for isolating specific lysogenic vibriophages.

Mitomycin C (Sigma Chemical Co., St. Louis, Mo.) was used for induction of lysogenic phages as per protocol described by Yee *et al.* (1993) with modifications. The filtrate was used as putative phage lysate to screen for plaque forming ability by double agar overlay method (Faruque *et al*. 1998). Tetrazolium staining (Pattee, 1966) helps to improve phage plaque visibility against the backdrop of the bacterial growth. Large scale production of phage lysate was

done by broth method as described by Faruque *et al*. (2005). Phage was concentrated using Polyethylene glycol (PEG) 6000 and DNA was isolated and analysed as described by Sambrook *et al*. (2000).

TEM analysis was done in high titer phage sample spotted onto a carbon-coated TEM grid, of Uranyl acetate (2%, pH 7.0) method (Luria *et al.*, 1943) was followed for TEM analysis of phage samples. The grids were dried for 3 h, examined and photographed using a Transmission Electron Microscope (Model JOEL JEM-100 X) operated at 80 KV at Indian Institute of Horticulture Research (IIHR) Hesaragatta, Bangalore. Phage morphology was analysed from the micrographs and the classification of phages was done in accordance with characteristics stated in the table.1

Table 1. Overview of phage families

Shape	Nucleic acid	Family	Genera	Example	Members
Tailed	dsDNA (L)	*Myoviridae*	6	T4	1,320
		Siphoviridae	7	λ	3,229
		Podoviridae	4	T7	771
Polyhedral	ssDNA (C)	*Microviridae*	4	*φX174*	40
	dsDNA (C, S)	*Corticoviridae*	1	PM2	3
	dsDNA (L)	*Tectiviridae*	1	PRD1	19
	dsDNA (L)	SH1∗		SH1	1
	dsDNA (C)	STIV∗		STIV	1
	ssRNA (L)	*Leviviridae*	2	MS2	39
	dsRNA (L, M)	*Cystoviridae*	1	*φ6*	3
Filamentous	ssDNA (C)	*Inoviridae*	2	M13	67
	dsDNA (L)	*Lipothrixviridae*	4	TTV1	7
	dsDNA (L)	*Rudiviridae*	1	SIRV-1	3
	dsDNA (C, S)	*Plasmaviridae*	1	L2	5
	dsDNA (C, S)	*Fuselloviridae*	1	SSV1	11
	dsDNA (L, S)	-	1∗∗	His1	1
	dsDNA (C, S)	*Guttaviridae*	1	SNDV	1
	dsDNA (L)	Ampullaviridae∗		ABV	1
	dsDNA (C)	Bicaudaviridae∗		ATV	1
	dsDNA (L)	Globuloviridae∗		PSV	1

C Circular; L linear; M multipartite; NC nucleocapsid; S supercoiled; _ no name;
∗Awaiting classification (adapted from Ackermann, 2009)

Results and Discussion

Vibrio cholerae isolates required as hosts for the isolation of the prophages, were isolated from marine environments like aquafarms and mangroves of Alappuzha and Ernakulam districts of Kerala, South India. Six isolates which were Gram negative, oxidase positive, fermentative, with or without gas production on MOF media and which showed yellow-coloured colonies on TCBS (Thiosulfate Citrate Bile salt Sucrose) agar were segregated as *Vibrio* sp.

Partial 16S rRNA gene was amplified and sequenced from 6 strains and their identity was confirmed by comparing the sequences in Genbank, by BLAST programme. The strains AR9, KNM4, KNM12, KNM20, MVN7 and MVN15 which showed 100% similarity with the classical virulent strains of *V. cholerae* were selected for further studies. The 16S rDNA partial gene sequences were deposited in the Genbank database. The Genbank accession number for AR9, KNM4, KNM12, KNM20, MVN7 and MVN15 are KJ734981, KJ734982, KJ734983, KJ734984, KJ734985 and KJ734986 respectively.

Twenty-two vibriophages were obtained from the *Vibrio cholerae* strains by induction with mitomycin C and were named appropriately as shown in table 2. Inducible prophages were also detected in the two standard virulent strains *V. cholerae* CO 336 and *V. cholerae* O139.

Table 2. Vibriophages obtained after induction of *V. cholerae strains* by Mitomycin C

Sl.No	strain	Source	Vibriophage	Strains producing plaques	
				Inductionwith mitomycin C	Without mitomycin C
1	**CO336 (Eltor strain)**	standard strain	Φ CO336	✓	x
2	**O139**	standard strain	Φ O139	✓	✓
3	**KNM4**	surface water	ΦKNM4	✓	✓
4	**KNM12**	surface water	ΦKNM12	✓	x
5	**MVN7**	mangroves	ΦMVN7	✓	x
6	**ALPVC3**	lab isolate	ΦALPVC3	✓	✓
7	**ALPVC4**	lab isolate	ΦALPVC4	✓	✓
8	**ALPVC5**	lab isolate	ΦALPVC5	✓	x
9	**ALPVC6**	lab isolate	ΦALPVC6	✓	x
10	**ALPVC7**	lab isolate	ΦALPVC7	✓	✓
11	**ALPVC8**	lab isolate	ΦALPVC8	✓	x
12	**ALPVC9**	lab isolate	ΦALPVC9	✓	✓
13	**ALPVC10**	lab isolate	ΦALPVC10	✓	✓
14	**ALPVC11**	lab isolate	ΦALPVC11	✓	x
15	**ALPVC12**	lab isolate	ΦALPVC12	✓	x
16	**ALPVC14**	lab isolate	ΦALPVC14	✓	✓
17	**EKM1**	lab isolate	ΦEKM1	✓	x
18	**EKM2**	lab isolate	ΦEKM2	✓	x
19	**EKM4**	lab isolate	ΦEKM4	✓	✓
20	**EKM6**	lab isolate	ΦEKM6	✓	x
21	**EKM7**	lab isolate	ΦEKM7	✓	x
22	**EKM8**	lab isolate	ΦEKM8	✓	x
23	**EKM10**	lab isolate	ΦEKM10	✓	x
24	**EKM14**	lab isolate	ΦEKM14	✓	✓

The strains that produced translucent plaques with bull's eye morphology on plating (Fig. 1) were identified as lysogen positive strains. A few strains; ΦALPVC3, ΦALPVC11, ΦALPVC12 and ΦEKM14 produced plaques even in control plates indicating spontaneous induction. These isolates which were

consistently induced with mitomycin C were morphological characterised using TEM.

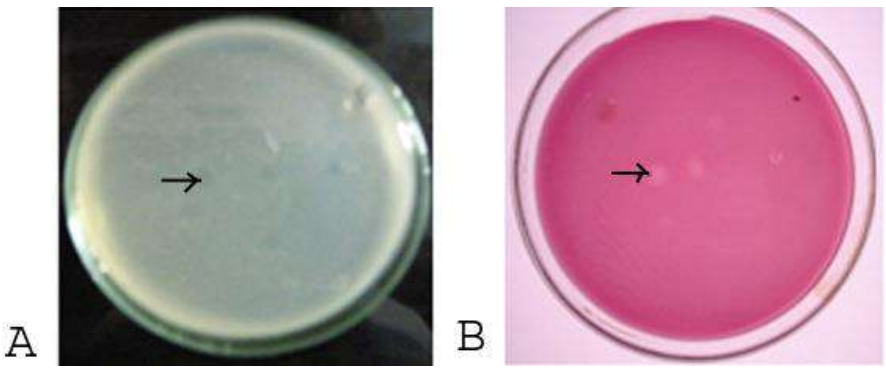

Figure 1. Assay for screening temperate phages.

A). Translucent plaques on double agar overlay assay
B). Tetrazolium-stained plates showing plaques formed by phage

The morphological features of bacteriophages greatly aid in their classification (Ackermann, 2009). Transmission electron microscopy was employed to elucidate the morphotype of phages. The TEM elucidated morphology has shown that the four phages studied belong to the three different double stranded DNA phage families, *i.e Myoviridae, Siphoviridae* and *Podoviridae*). ΦALPVC3 which was T4-like was a myovirus; ΦALPVC11 and ΦALPVC12 were siphophages and λ-likephages), and ΦEKM14 was a podophage.

TEM image of ΦALPVC 3 (Figure 2 A) exhibited isometric or elongated head with a diameter of 65 ± 0.50nm and long tail of 75 ± 0.25nm. A few tail fibers or spikes were also noticed. The TEM pictures of ΦALPVC11 and ΦALPVC12 (Figure 2.B and 2.C) show bacteriophages with thin long and flexible tails with icosahedral or prolate virion, which is typical for siphovirus.

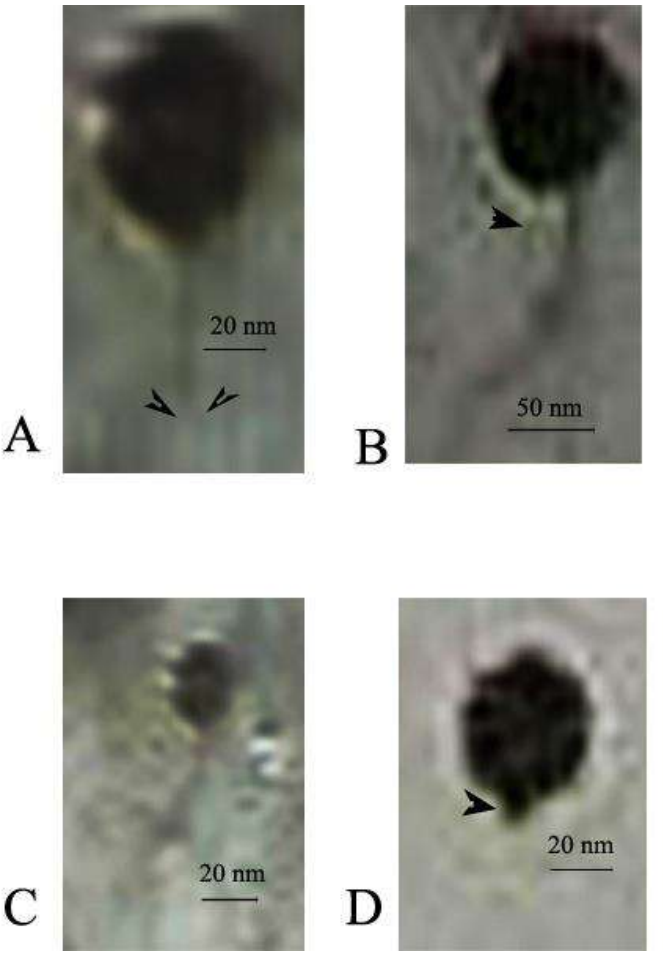

Fig. 2. Transmission Electron micrograph image of phage stained with 1% uranyl acetate

A) ΦALPVC3 with tail fibres (arrows) B) ΦALPVC11 with apical protrusions on head (arrow) C) ΦALPVC12 D) ΦEKM14 with short tail fibres (arrow)

Phage dimensions as observed from the micrographs were as follows- ΦALPVC11 showed 62 ± 0.20 nm head and 159 ± 0.25 nm long tail and that of ΦALPVC12 are 30 ± 0.50 nm (head) and 84 ± 0.40 nm (tail). The vibriophage ΦALPVC11 was also found to have apical protrusions on the head. The two phages in *Siphoviridae* family thus belonged to two different morphological types. ΦEKM14 (Figure 2.D), the podophage was distinguished by short non-

contractile tail (12± 0.32 nm) and icosahedral head (44 ± 0.38 nm) which was typical of T-7 like- phages. The phage sizes were determined from the average of 3 independent measurements (mean ± standard deviation).

Vibriophages with similar morphology were previously reported (Sen and Ghosh, 2005). Ackermann and DuBow, (1987) reported two non-cultivated rumen bacteriophages with such long tails as seen in ΦALPVC11. It is also reported that the average head diameter for phages of family *Siphoviridae* is 62.5 nm with 120nm long tail (De Lappe *et al.,* 2009). Bacteriophage ΦEKM14 is a podophage similar to the N5 vibriophage (Sen and Ghosh, 2005) showing an isomeric head with an extremely short non-contractile tail. It is reported that the average head diameter is 62.5 nm and tail length 13nm for phages belonging to family *Podoviridae* (De Lappe *et al.,* 2009). *Podoviridae* bacteriophages have also been previously reported (Kropinski *et al*., 2007).

Conclusion

Horizontal gene transfer is considered as the most possible event for transition of environmental vibrio in to virulent vibrios. The presence of inducible prophages in the environmental isolates of *V. cholerae* can be used as a surveillance mechanism for cholera outbreak. The morphology and classification of the phages is also a determining factor for gene transfer.

Acknowledgement

This study was supported by Department of Biotechnology, Cochin University of Science and Technology, Cochin, Kerala, India. The first author gratefully acknowledges the IIHR, Bangalore for the research facilities provided for TEM.

References

Ackermann, H. W. (2007) 5500 Phages examined in the electron microscope. *Archives of virology*. 152(2): 227-243.

Ackermann, H. W. (2009). Basic phage electron microscopy. In *Bacteriophages* (pp. 113-126). Humana Press.

Ackermann, H. W. and DuBow, M. S. (1987). Viruses of prokaryotes, vol. 2. *Natural groups of bacteriophages*. (pp. 145-167). Humana Press.

Bik, E. M., Bunschoten, A. E., Gouw, R. D. and Mooi, F. R. (1995) Genesis of the novel epidemic *Vibrio cholerae* O139 strain: evidence for horizontal transfer of genes involved in polysaccharide synthesis. *The EMBO journal*. 14(2): 209.

Bradley, D. E. (1967). Ultrastructure of bacteriophage and bacteriocins. *Bacteriological reviews*. 31(4): 230.

Colwell, R. R. (1996). Global climate and infectious disease: the cholera paradigm. *Science.* 274(5295): 2025-2031.

Davis, B. M. and Waldor, M. K. (2003) Filamentous phages linked to virulence of *Vibrio cholerae*. *Current opinion in microbiology.* 6(1): 35-42.

De Lappe, N., Doran, G., O'Connor, J., O'Hare, C. and Cormican, M. (2009) Characterization of bacteriophages used in the Salmonella enterica serovar Enteritidis phage-typing scheme. *Journal of medical microbiology*. 58(1): 86-93.

Faruque, S. M., Alim, A. A., Albert, M. J., Islam, K. N. and Mekalanos, J. J. (1998) Induction of the lysogenic phage encoding cholera toxin in naturally occurring strains of toxigenic *Vibrio cholerae* O1 and O139. *Infection and immunity*. 66(8): 3752-3757.

Faruque, S. M., Chowdhury, N., Kamruzzaman, M., Dziejman, M., Rahman, M. H., Sack, D. A. and Mekalanos, J. J. (2000) Genetic diversity and virulence potential of environmental *Vibrio cholerae* population in a cholera-endemic area. *Proceedings of the National Academy of Sciences of the United States of America*. 101(7): 2123-2128.

Faruque, S. M., Naser, I. B., Fujihara, K., Diraphat, P., Chowdhury, N., Kamruzzaman, M. and Mekalanos, J. J. (2005) Genomic sequence and receptor for the Vibrio cholerae phage KSF-1Φ: evolutionary divergence among filamentous vibriophages mediating lateral gene transfer. *Journal of bacteriology*. 187(12): 4095-4103.

Geeta, M. G. and Krishnakumar, P. (2005) Cholera in Kerala. *Indian Pediatrics Journal*. 42: 89.

Goyal, S. M., Gerba, C. P. and Bitton, G. (1987) Phage ecology. *Wiley series in ecological and applied microbiology (USA).*

Jiang, S. C. and Paul, J. H. (1998) Gene transfer by in marine environment. *Applied and Environmental Microbiology*. 64(8): 2780-2787.

Kar, S., Ghosh, R. K., Ghosh, A. N., & Ghosh, A. (1996) Integration of the DNA of a novel filamentous bacteriophage VSK from *Vibrio cholerae* 0139 into the host chromosomal DNA. *FEMS microbiology letters.* 145(1): 17-22.

Kropinski, A. M., Sulakvelidze, A., Konczy, P. and Poppe, C. (2007) Salmonella phages and prophages-genomics and practical aspects. In *Salmonella* (pp. 133-175). Humana Press.

Luria, S. E., Delbrück, M. and Anderson, T. F. (1943) Electron microscope studies of bacterial viruses. *Journal of bacteriology*. 46(1): 57.

Ogg, J. E., Timme, T. L. and Alemohammad, M. M. (1981) General transduction in *Vibrio cholerae*. *Infection and immunity*. 31(2): 737-741.

Sambrook, J., Fritish, E. and Maniatis, I. (2000) Molecular Cloning, a Laboratory manual. In 3 (Ed.), C.S.H. Laboratory, Ed.

Sen, A. and Ghosh, A. N. (2005) New *Vibrio cholerae* O1 biotype ElTor bacteriophages. *Virology journal.* 2(1): 28.

Shivaji, S., Vijaya Bhanu, N. and Aggarwal, R. K. (2000) Identification of *Yersinia pestis* as the causative organism of plague in India as determined by 16S rDNA sequencing and RAPD-based genomic fingerprinting. FEMS Microbiology Letters. 189 (2): 247-252.

Waldor, M. K., & Mekalanos, J. J. (1994) Emergence of a new cholera pandemic: molecular analysis of virulence determinants in *Vibrio cholerae* 0139 and development of a live vaccine prototype. *Journal of Infectious Diseases*. 170(2): 278-283.

Waldor, M. K., & Mekalanos, J. J. (1996). Lysogenic conversion by a filamentous phage encoding cholera toxin. *Science*. 272(5270): 1910-1914.

Yee, A. J., De Grandis, S. and Gyles, C. L. (1993) Mitomycin-induced synthesis of a Shiga-like toxin from enteropathogenic *Escherichia coli* HI 8. *Infection and immunity*. 61(10): 4510-4513.

BIOSURFACTANTS FROM PIGMENTED YEASTS ISOLATED FROM MANGROVES OF CENTRAL KERALA AND ITS APPLICATION

K. A. Nimsi[1], K. Manjusha[1*], N. Nefla[2], S. N Kutty[3] and V.S. Aneymol[4]

[1]Faculty of Ocean Science and Technology, Kerala University of Fisheries and Ocean Studies, Panangad, Kerala, India
[2]Department of Microbiology, St. Xavier's College for Women, Aluva, Kerala
[3]Department of Zoology, N.S.S. College, Nenmara, Palakkad, Kerala
[4]Department of Microbiology, St. Xavier's College for Women, Aluva, Kerala
[*]**Corresponding Author Email id:** manjusha.k@kufos.ac.in or manjushak.kufos@gmail.com

Abstract

In the last few years synthetic surfactants have become increasingly unpopular as they are not eco-friendly and entirely safe for human use. This has led to an intensification of the search for biological sources of surfactants as they are biodegradable and have low toxicity. Microbes are a predominant source of biosurfactants. Though bacteria have been identified as significant producers of biosurfactants, they have been found to be potentially pathogenic and this has led to a shift in interest in biosurfactant-producing yeasts and yeast-like fungi. Yeasts from ecosystems like mangroves are not fairly reported for biosurfactant production. Thus, the present study aimed to study the biosurfactant-producing pigmented yeasts from the mangroves in Central Kerala. Seven morphologically distinct pigmented isolates (MA19, MUL 30, PV56, PV77, VA115, PV148, and VA242) were selected for the study. Oil displacement, Parafilm test, and emulsification index results revealed that the isolate VA 242 had maximum biosurfactant activity. The biosurfactant from the strain VA242 was extracted and concentrated. Biochemical characterization of the biosurfactant of VA242 indicated that it was glycolipid in nature. The purified biosurfactant exhibited both antimicrobial and strong antioxidant activity. The visual monitoring of the cleaning efficacy of biosurfactant was comparable to commercially available surfactant SDS. The study clearly indicated that the yeast *Rhodotorula paludegina* VA 242 is a promising source of biosurfactant with the potential to be employed in the pharmaceutical and detergent industry.

Keywords: Yeast, Biosurfactant, Emulsification index, Glycolipid, Mangrove, Pigment

Introduction

Biosurfactants have stirred up the interest of the scientific community in recent years due to several advantages they possess over synthetic counterparts namely biodegradability, selectivity, stability in a range of conditions, and low toxicity Biosurfactants find application in the recovery of hydrophobic compounds and emulsifiers in the pharmaceutical, cosmetic, and food industries (Garg and Priyanka, 2018; Felix *et al.*, 2018).

In terms of volume of data and scientific output, bacterial biosurfactants lead the list of microbial surfactants. Bacterial biosurfactants are mainly reported from *Pseudomonas* and *Bacillus* strains (da silva *et al.,* 2018). However, these bacterial genera are not safe for industrial use. Though fungal biosurfactants, in comparison, represent only 19% of the total biosurfactants they are found to have the most chemical and structural versatility. Among fungi, yeasts have been identified as an ideal source as they are GRAS (Generally Recognized as Safe) and highly versatile in terms of their chemical structure (Desai and Banat, 1997). Biosurfactant production by yeast has been reported mainly from *Yarrowia* sp., *Pseudozyma* sp., and *Candida* sp. (Fontes, 2008).

The industry is in a constant search for newer sources of biosurfactants with novel surface and emulsifying activities. A promising niche for isolating biosurfactant-producing yeasts is mangrove ecosystems. Therefore, the main aim of this work was to investigate the potential of biosurfactants obtained from manglicolous yeasts isolated from Kerala.

Materials and Methods

(a) Strains used

Seven morphologically distinct pigmented yeasts strains (MA19, MUL 30, PV56, PV77, VA115, PV148, and VA242) isolated as a part of the Kerala State

Council for Science Technology and Environment funded project 'Diversity and Biotic Potential of Yeasts from the Mangroves of Central Kerala', were selected for this study.

(b) Preinoculum

To check for biosurfactant production capability the selected pigmented isolates (MA19, MUL 30, PV56, PV77, VA115, PV148, and VA242) were inoculated into 10 ml of YM (glucose 1g, malt extract 0.3g, peptone 0.5g, yeast extract 0.3g, seawater 100 ml) media and incubated for 7 days in a rotary shaker for 120 rpm at 30ºC or 7 days. This served as a pre-inoculum.

(c) Production

Biosurfactant production was carried out in the modified YM broth (glucose was replaced with 1% diesel as the carbon source). Modified YM broth (100 ml) was inoculated with 10 ml of pre-inoculum. The inoculated tubes were incubated for 7 days in a rotary shaker for 120 rpm at 30ºC. After incubation, the 7 days cultures were centrifuged at 8000 rpm for 15 minutes and the pellet was decanted. The supernatant was collected for physio-chemical characterization

- **Physical characterization**

Parafilm test

Fifty microliters of the culture supernatant were placed on the strip of Parafilm M and the diameter was noted. The shape of the supernatant drop on the surface of parafilm M was examined after 1min. If the drop becomes flat, it indicates the presence of biosurfactant in the supernatant. If the drop retains the dome shape, it indicates a negative result (Patel and Patel, 2020).

Oil displacement test

Thirty milliliter of distilled water and 50 µl of oil (sunflower oil, olive oil, mustard oil, coconut oil and gingelly oil, and diesel) were taken in a Petri plate.

Supernatant (50 µl) was added to the center of the oil. The diameter of the zone of displacement on addition of supernatant was measured as a measure of biosurfactant production (Patel and Patel, 2020).

Emulsification index measurement

To determine the Emulsification index, 4ml diesel was added to 4ml of culture supernatant, vortexed for 2 minutes, and allowed to stand for 24hr.The emulsification index was calculated using the formula,

E 24= Height of emulsification layer / Total height x100

- **Chemical characterization**

Phenol sulphuric acid test

One ml of 5% phenol was added to 1ml cell-free culture supernatant. To this mixture, 4 drops of concentrated H_2SO_4 were added. The development of orange color on the addition of reagent indicates the presence of glycolipids (Kalyani and Sireesha, 2014).

Biuret test

Two ml of cell-free culture supernatant was heated at 70º C for 10 minutes and 10 drops of 1M NaOH was added to this. To this mixture, 1% Copper sulphate solution was added drop by drop. The appearance of a violet or pink ring indicates the presence of lipopeptides.

Phosphate test

To 2ml of culture supernatant 10 drops of 6M Nitric acid were added and heated at 70ºC for 10 minutes. Yellow color development after the addition of 5% ammonium molybdate solution is indicative of the presence of phospholipids.

- **Biosurfactant recovery from VA 242**

Biosurfactant from the most potent producer VA 242 was extracted. For this, the culture broth was centrifuged at 10,000 rpm for 10 min and the supernatant was collected in a beaker. One molar H_2SO_4 was used to adjust the pH of the supernatant to 2 (Muthezhilan *et al.,* 2014). To this supernatant chloroform: methanol (2:1) was added and kept in a beaker overnight covered with aluminium foil with holes in it. On evaporation of the solvent, the biosurfactant precipitated as a white-colored powder (Sekar *et al.,* 2010)**.**

- **Applications of biosurfactant from VA 242**

Antimicrobial activity

The extracted biosurfactant was dissolved in sterile distilled water and the antimicrobial activity was checked against bacterial pathogens *Escherichia coli*, *Pseudomonas* sp., *Bacillus* sp., *Vibrio* sp., *Aeromonas* sp., *Salmonella* sp., *Klebsiella* sp., *and Staphylococcus* sp. by disc diffusion method. Sterile discs (Himedia) were impregnated with biosurfactant at a concentration of 1mg/ml (20µl). The impregnated discs were placed on test cultures swabbed onto Muller Hinton Agar and incubated for 24 hrs at 37ºC. SDS and water were taken as positive and negative control respectively.

Antioxidant activity

For the antioxidant assays, the powdered extract was dissolved in water, to prepare various concentrations (20, 40, 60, 80, and 100 µg/ml) and assayed for antioxidant activity. All experiments were conducted in triplicates. The antioxidant activity of VA 242 biosurfactant was determined using Diphenyl-2-picrylhydrazyl (DPPH) scavenging activity (DPPH) assay and 2, 2'-Azino-Bis-3-Ethylbenzothiazoline-6-Sulfonic Acid (ABTS) radical assay (Mukherjee *et al.,* 2017).

Application as detergent additive

Clean white cotton fabric was cut into three pieces (5 × 5 cm) that were stained with motor oil. The stained fabric samples were immersed in an aqueous solution of i) biosurfactant (1.5%) this served as Test (T), ii) Sodium Dodecyl Sulphate (SDS)- positive control (P) and iii) untreated fabric was the negative control (N). The fabric was washed by placing the flask containing the fabric and water in rotary shaker at a speed of 160 rpm for 1 hr. After washing cotton fabric was rinsed twice with 50 mL of distilled water for 30 min (at 120 rpm) followed by drying at room temperature (Bouassida *et al.*, 2018).

Results and Discussion

All the selected pigmented (MA 19, MUL 30, PV77, PV56, VA 115, PV148, and VA 242) isolates when screened for biosurfactant production by Parafilm test, Oil displacement and emulsification index method were found to produce biosurfactant (Figure 1). However, the maximum diameter of the drop on parafilm as well as maximum oil displacement activity was exhibited by the biosurfactant from VA 242. Except for the biosurfactants from VA 242 and MUL 30, none of the others were able to displace coconut oil (Table 1). The greatest emulsification index value of 49.7 % was also exhibited by VA 242 followed by MUL 30 (37.81%) and MA19 (33.21%) (Table 2).

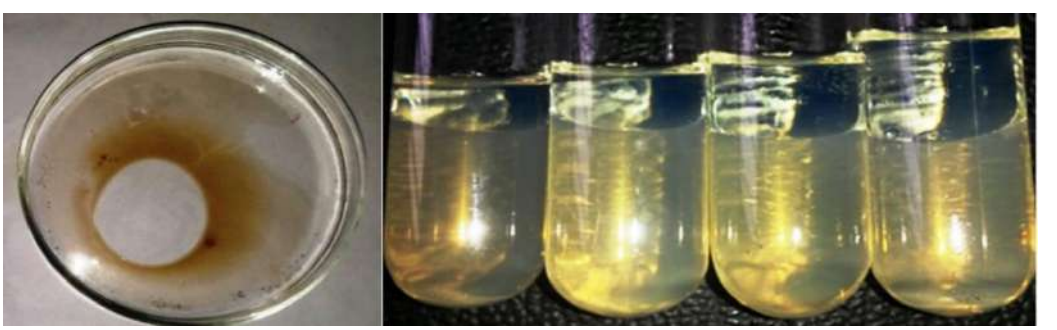

Figure 1. Oil displacement and Emulsification index

Table 1. Oil displacement by the biosurfactants produced by pigmented yeasts

Isolates	Diesel	Olive oil	Coconut oil	Sunflower oil	Gingelly oil	Mustard oil
242	32 mm	34 mm	11 mm	26 mm	19 mm	23 mm
19	18 mm	21 mm	-	11 mm	10 mm	15 mm
30	21 mm	11 mm	10 mm	23 mm	15 mm	21 mm
56	10 mm	20 mm	-	18 mm	10 mm	10 mm
77	26 mm	31 mm	-	20 mm	10 mm	20 mm
115	20 mm	19 mm	-	15 mm	14 mm	18 mm
148	30 mm	29 mm	-	22 mm	10 mm	10 mm

Table 2. Physico –chemical characteristics of the biosurfactants

Isolates	parafilm	Emulsification index	Phenol H_2SO_4	Biuret	phosphatase
242	5 mm	49.7%	+	-	-
19	4 mm	33.21%	+	-	-
30	4 mm	37.81%	-	+	-
56	2 mm	27.01%	+	-	-
77	3 mm	28.91%	-	+	-
115	2 mm	26.67%	+	-	-
148	4 mm	31.67%	+	-	-

The results of the physico-chemical characterization of the yeast biosurfactants have been summarized in table 2. Phenol-Sulfuric acid test, Biuret test, and Phosphate test were performed with cell-free supernatant to identify the type of biosurfactant produced. The biosurfactant from MA 19, PV56, VA 115, PV148, and VA 242 answered the phenol H_2SO_4 test therefore was identified as a glycolipid. Whereas, the biosurfactants from MUL 30 and PV 77 answered the Biuret test indicating that they were lipopeptides. It is clear from this study that the biosurfactants from mangrove yeasts were of varied chemical nature. Glycolipids are potential bio-molecules for use in the food and pharmaceutical industry (Ribeiro *et al.*, 2020).

The most potent isolate VA242 was identified as *Rhodotorula paludigena* previously (Rekha *et al.,* 2022). The biosurfactant from the potential stain 242 was extracted and various areas of its possible application were evaluated. The

antimicrobial activity of the biosurfactant was checked against various bacterial pathogens and was found to have the ability to inhibit all microbial cultures tested to a varying degree. The results are shown in table 3. It exhibited a maximum zone of inhibition against *A. hydrophila* (Figure 2).

Table 3. Antibacterial activity of biosurfactant from VA 242

Sl No	Organisms	Antimicrobial activity of SDS	Antimicrobial activity of Biosurfactant synthezised by VA 242
1	*B.cereus*	2 mm	8 mm
2	*V. alginolyticus*	4 mm	7 mm
3	*V. proteolyticus*	-	9 mm
4	*V.fluvinalis*	-	8 mm
5	*P.aeroginosa*	-	10 mm
6	*E.tarda*	5 mm	5 mm
7	*V.harveyi*	5 mm	5 mm
8	*A.hydrophilla*	6 mm	15 mm
9	*S.aureus*	-	13 mm
10	*V.vulnificus*	-	11 mm
11	*V.cholerae*	-	12 mm
12	*V.parahaemolyticus*	-	12 mm
13	*E.coli*	9 mm	9 mm
14	*Salmonella*	8 mm	10 mm
15	*Klebsiella*	-	11 mm

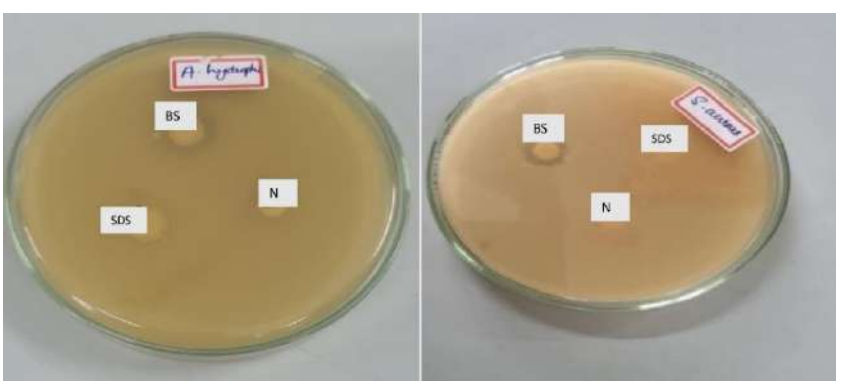

(a) **(b)**

Figure 2. Antibacterial activity of extracted biosurfactant (a) *A. hydrophilla (b) S. aureus*

The biosurfactant from *Rhodotorula paludigena* also exhibited strong antioxidant activity this was found to be concentration-dependent. At a concentration of 100µg/ml the biosurfactant displayed 89 % antioxidant activity by DPPH analysis and 95% by ABTS assay. The percentage of inhibition was comparable to the chemical surfactant SDS (Figure 3). Thus, the biosurfactant from VA242 can be used as an antioxidant ingredient in food formulations.

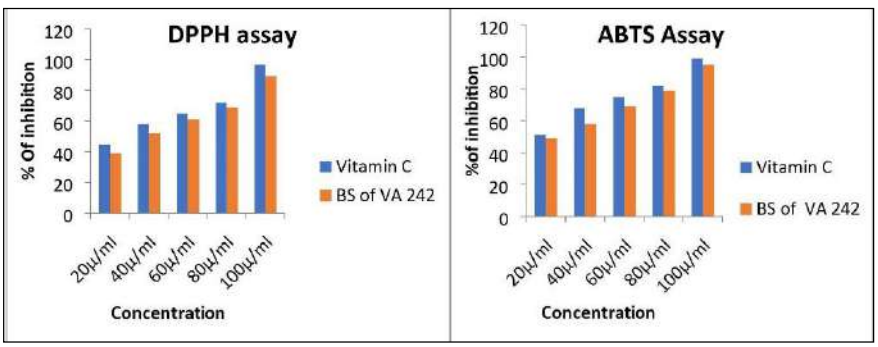

Figure 3. Antioxidant activity of biosurfactant

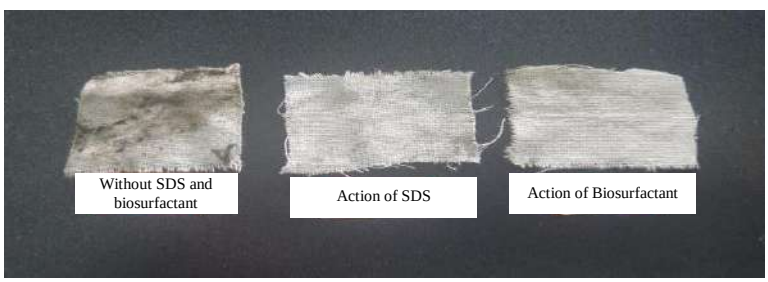

Figure 4. Washing efficacy of biosurfactant and SDS

The visual monitoring of the cleaning efficacy of the biosurfactant was comparable to that of the commercially available surfactant SDS (Figure 4). An advantage of this biosurfactant over commercial detergent is that it is able to clean and degrease even in the absence of the ingredients of a detergent. Biosurfactant demands have spiked in recent years therefore the isolate *Rhodotorula paludigena* VA 242 has great industrial potential.

Conclusion

The findings of present study reveal that the glycolipid biosurfactant from GRAS organism *Rhodotorula paludigena* VA 242, has both antioxidant and antibacterial activity which opens the door for its possible application in the pharma industry. The efficacy of the biosurfactant in removing motor oil stains also opens the possibility of its application in the detergent industry. Further study of this strain and optimization of conditions for its production can lead to an effective microbial biosurfactant that can be applied in the industry as a safe alternative to synthetic surfactants.

Acknowledgement

The authors gratefully acknowledge the financial support by the The Kerala State Council for Science, Technology and Environment (KSCSTE) for the project entitled 'Diversity and Biotic Potential of Yeasts from the Mangroves of central Kerala' (Order No .573/2017/KSCSTE DTD 03/10/2017).

References

Adetunji, A. I., and Olaniran, A. O (2021) Production and potential biotechnological applications of microbial surfactants: An overview. *Saudi Journal of Biological Sciences.* 28(1): 669-679.

Bouassida, M., Fourati, N., Ghazala, I., Ellouze-Chaabouni, S. and Ghribi, D (2018) Potential application of Bacillus subtilis SPB1 biosurfactants in laundry detergent formulations: compatibility study with detergent ingredients and washing performance. *Engineering in Life Sciences*. 18(1): 70-77.

Çelik, P. A., Manga, E. B., Çabuk, A and Banat, I. M (2020) Biosurfactants' potential role in combating COVID-19 and similar future microbial threats. *Applied Sciences*. 11(1): 334.

Da Silva, A. C. S and Dos Santos, P. N (2018) E Silva, TAL; Andrade, RFS; Campos-Takaki, G. Biosurfactant production by fungi as a sustainable alternative. *Arquivos do Instituto Biol*ogico. *85*: 1808-1657000502017.

da Silva, A. F., Banat, I. M., Giachini, A. J and Robl, D (2021) Fungal biosurfactants, from nature to biotechnological product: bioprospection, production and potential applications. *Bioprocess and Biosystems Engineering.* 44(10): 2003-2034.

Desai, J. D and Banat, I. M (1997) Microbial production of surfactants and their commercial potential. *Microbiology and Molecular biology reviews*. 61(1): 47-64.

Felix, A. K. N., Martins, J. J., Almeida, J. G. L., Giro, M. E. A., Cavalcante, K. F., Melo, V. M. M., ... and de Santiago Aguiar, R. S. (2019) Purification and characterization of a biosurfactant produced by Bacillus subtilis in cashew apple juice and its application in the remediation of oil-contaminated soil. *Colloids and Surfaces B: Biointerfaces*. 175*:* 256-263.

Fontes, G. C., Amaral, P. F. F and Coelho, M. A. Z (2008) Produção de biossurfactante por levedura. *Química Nova*. 31: 2091-2099.

Garg, M and Chatterjee, M (2018. Isolation, characterization and antibacterial effect of biosurfactant from Candida parapsilosis. *Biotechnology Reports.* 18: e00251.

Inès, M. and Dhouha, G (2015) Glycolipid biosurfactants: Potential related biomedical and biotechnological applications. *Carbohydrate Research.* 416: 59-69.

Kalyani, A. L. T and Sireesha, G. N (2014) Isolation of bio-surfactant producing actinomycetes from terrestrial and marine soils.

Mukherjee, A. K and Das, K (2010) Microbial surfactants and their potential applications: an overview. *Biosurfactants*. 54-64.

Muthezhilan, R., Ragul, R., Pushpam, A. C and Hussain, A. J (2014) Production and purification of biosurfactant from marine yeast isolated from kelambakkam salterns. *Biosciences Biotechnology Research Asia.* 11: 59-67.

Patel, K and Patel, F. R (2020) Screening of biosurfactant producing yeasts isolated from mangrove ecosystem of Surat region of Gujarat, India. Indian Journal of Science and Technology. 13: 204.

Ribeiro, B. G., Guerra, J. M. C and Sarubbo, L. A (2020) Potential food application of a biosurfactant produced by Saccharomyces cerevisiae URM 6670. *Frontiers in Bioengineering and Biotechnology.* 8: 434.

Satpute, S. K., Banpurkar, A. G., Dhakephalkar, P. K., Banat, I. M and Chopade, B. A (2010) Methods for investigating biosurfactants and bioemulsifiers: a review. *Critical reviews in biotechnology*. 30(2): 127-144.

Sekar, K. V., Kumari, S., Nagasathya, A., Palanivel, S and Nambary, S (2010) Effective biosurfactants production by Pseudomonas aeruginosa and its efficacy on different oils. *Journal of advanced laboratory research in Biology*. 1(1): 40-44.

MOLECULAR DOCKING COMPARATIVE STUDIES OF SOME POTENT HOME REMEDIES AND COMMERCIAL DRUGS FOR MOTION SICKNESS

K.A Stella[1]*, Rini Simon[2] and E P Vineetha[3]

[1&2]Department of Chemistry, St. Xavier's College for Women, Aluva, Ernakulam, Kerala, India
[3]Department of Physics, St. Xavier's College for Women, Aluva, Ernakulam, Kerala, India
***Corresponding Author email id:** stellagrace@stxaviersaluva.ac.in

Abstract

The binding affinity of various commercially available drugs, such as Cyclizine, Promethazine, Zofran, Granisetron, and other drugs present in suggested home remedies for motion sickness, such as D-limonene (Lemon), Menthol (Mint), Cumin oil, Ginger (*Zingiber officinale*) on different receptors like the target protein- H1histamine receptor and 5HT3 serotonin receptor were studied using molecular docking method. Some of the properties of these drugs, like drug-likeness, were also analyzed using SWISS –ADME online software.

Keywords: Drug-receptor interaction, motion sickness, molecular modelling, home remedies

Introduction

Motion Sickness or travel sickness is caused by various motions such as traveling in vehicles, boats, planes, etc., and its well-known symptoms include nausea, vomiting, and headache. The reason for motion sickness is the difference between actual and expected motion (Hromatka *et al*., 2015; Ray, 2018). The vestibular system of the inner ear senses the position of the body and its movements and also influences the balance, 'signals' moving' to the brain. The viewer experiences a stationary effect of the car or boat at the time of its motion

(Hromatka *et al*., 2015; Ray, 2018). This motion sickness is also called kinetosis, and many have experienced motion sickness in her or his lifetime. Females are more susceptible to motion sickness than males of the same age in terms of increased frequency and severity of symptoms, especially during menstruation. During pregnancy, hormonal changes make women susceptible to this sickness (Leung and Hon, 2019).

The evaluation and prediction of motion sickness have been tested using different physiological measures. Yet no single parameter is of enough sensitivity and specificity for diagnosing or predicting individual motion sickness susceptibility. The initial symptom is discomfort around the upper abdomen ("stomach awareness"), which is followed by nausea and increasing malaise (Shupak and Gordon, 2006). Diagnosing motion sickness is easy because it is visible outside through evident symptoms (Koch *et al.*, 2018). Drugs that are mainly used for motion sickness belong to the antiemetics class of drugs. They are drugs that are effective against vomiting and nausea, which are major symptoms of motion sickness. They are of different types, such as 5-HT3 receptor antagonists, dopamine antagonists, NK1 receptor antagonists, antihistamines, cannabinoids, anticholinergics, steroids, and many others. Antihistamines- H1 Histamine receptor antagonists- are effective in many conditions of motion sickness, even during pregnancy. H1 receptors in central areas include area postrema and vomiting center in the vestibular nucleus, which also has anticholinergic drug properties that block some other receptors too. Cyclizine and promethazine are two important drugs that are commercially available. 5-HT3 receptor antagonists block serotonin receptors in the Central nervous system and gastrointestinal tracts. They are also used against vomiting and nausea. Ondansetron (Zofran) and Granisetron are commercially available drugs in this class. Both these drugs can be administered orally or intravenously.

But these drugs are also marked with side effects like constipation, diarrhea, dry mouth, and fatigue (Koch *et al.*, 2018).

But it is commonly said that there are certain home remedies too for motion sickness. For example, Ginger (*Zingiber officinale*) is said to be good for stomach upset, motion sickness, nausea, vomiting, etc. Similarly, it is suggested that while traveling, if people tend to vomit, the smell of cumin seeds, lemon, or some mint leaves can reduce this feeling. Lemon contains D-limonene, and menthol is present in mint, giving it a special smell. So, whether these home remedies can bind the receptors in the same way as antiemetic drugs is studied through these molecular modelling methods. SWISS-ADME software helps analyse the properties of these drugs like drug-likeness by looking at whether it satisfies Lipinski's rule, solubility, medicinal effects, etc.

Materials and Methods

Step 1- Preparing the ligand (drug) for docking.

Drug structures for all the drugs taken to study, such as D-limonene, Menthol, Cumin oil, Ginger (Zingiber officinale), Cyclizine, Promethazine, Zofran, and Granisetron are downloaded from the PubChem database in SDF format. It is then converted into the PDB format using open babel software. Information regarding the properties of these drugs is obtained by using online SWISS-ADME software, copying the smiles from the database to the SWISS-ADME input smile area, and pressing the run button.

Step 2 -Preparing the receptor (protein) for docking.

Protein structures of H1 and 5HT3 receptors are downloaded from RSC Protein Data Bank in PDB format. Then by using pyMol software, the water molecules and other residues are removed, and valence corrections are made by adding H atoms.

Step 3- Docking of prepared ligand and protein.

Using autodock software, the macromolecule (protein) and ligand (drug) are loaded and converted to pdbqt format. This step is repeated for every drug and receptor. The grid box was set on the macromolecule, and using the grid parameters; a conf.txt file was prepared. After this, docking calculations were carried out for each set using the command prompt "vina-config conf.txt." The binding energy is obtained in this program run. Now using the discovery studio software, the macromolecule is loaded, and the output file of autodock is dragged into the discovery studio window. From there, the ligand macromolecule interactions can be viewed. This is repeated for each drug. Results obtained are compared to understand whether home remedies are beneficial, just like commercially available drugs.

Results and Discussions

The binding affinity of drugs present in four selected home remedies, such as lemon, mint leaves, cumin, ginger, and two commercial drugs cyclizine and promethazine on H1 (Histamine receptor) protein is compared and is given in Figure 1.

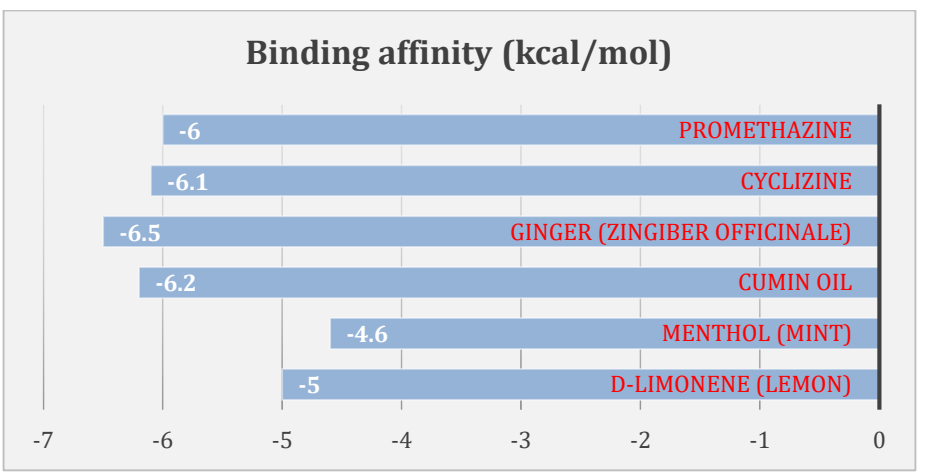

Figure 1. Binding Affinity of Drugs on H1 Receptors

The binding affinity of D-Limonene (lemon) and Menthol (mint) on H1 histamine receptor was deficient. So, these home remedies do not have much effect on this receptor. Furthermore, on analysing commercial drug binding affinity, Cyclizine has a binding affinity of-6.1kcal/mol, and promethazine has -6.0 kcal/mol. Compared to these values, an astonishing result is seen for cumin and ginger because these drugs show binding affinity values of –6.2kcal/mol and -6.5 kcal/mol, respectively. The results show that these home remedies have a greater binding affinity than the commercially available drugs with this receptor. The interaction of H1 receptor with D- Limonene, Menthol, Cumin, Ginger, Cyclizine, and promethazine are shown in Figures 2,3,4,5,6,7 respectively.

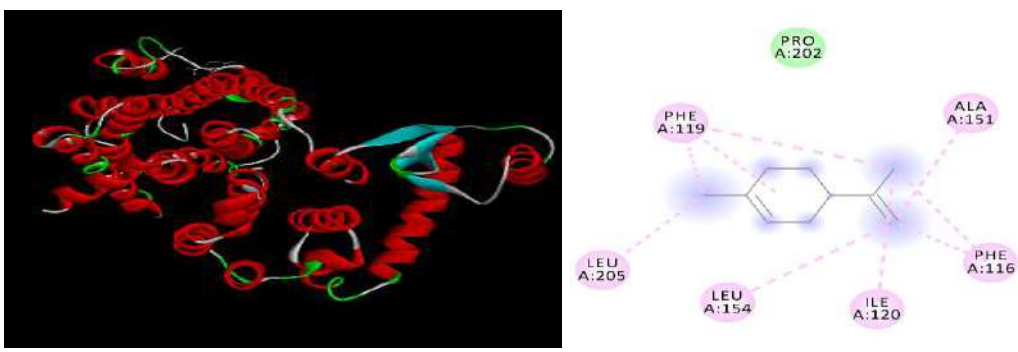

Figure 2. Interaction of D-Limonene (Lemon) with H1 Receptor

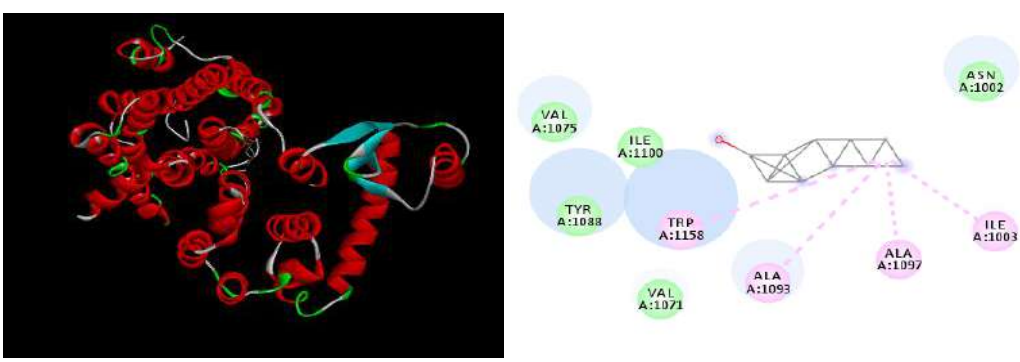

Figure 3. Interaction of Menthol (Mint) with H1 Receptor

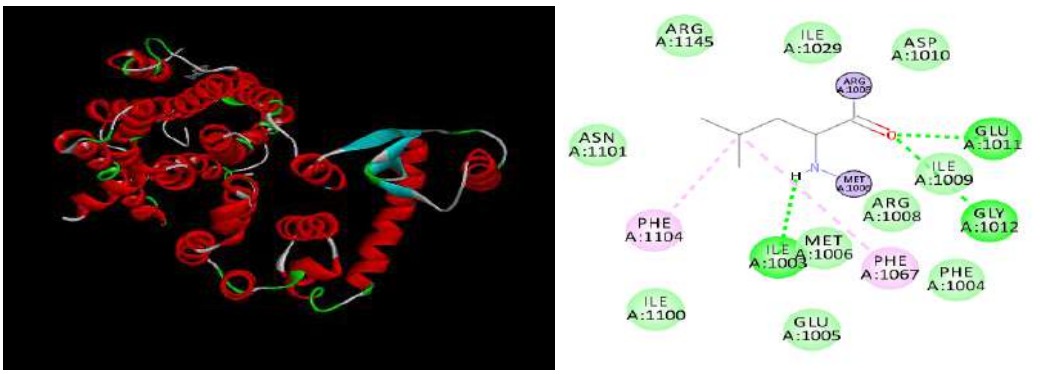

Figure 4. Interaction of Cumin Oil with H1 Receptor

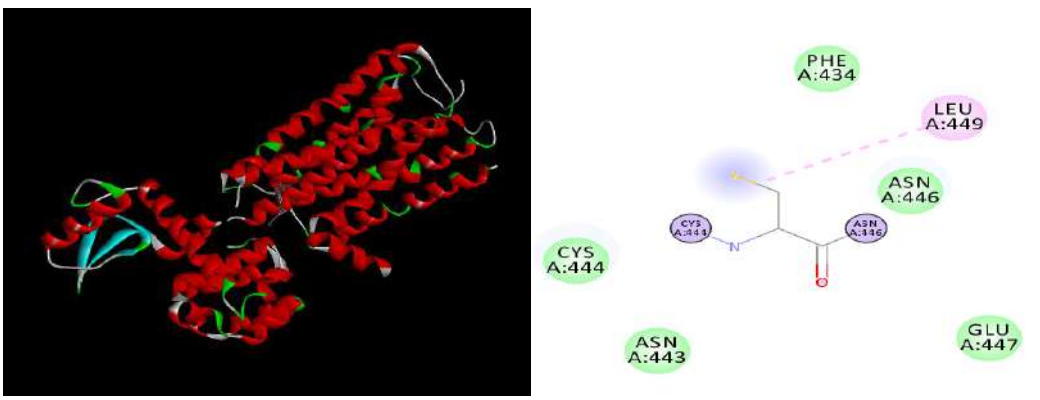

Figure 5. Interaction of Ginger (*Zingiber officinale*) withH1 Receptor

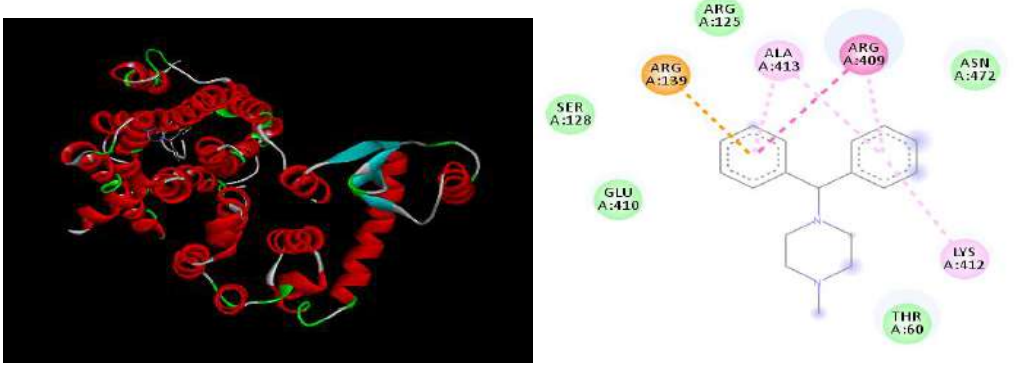

Figure 6. Interaction of Cyclizine with H1 Receptor

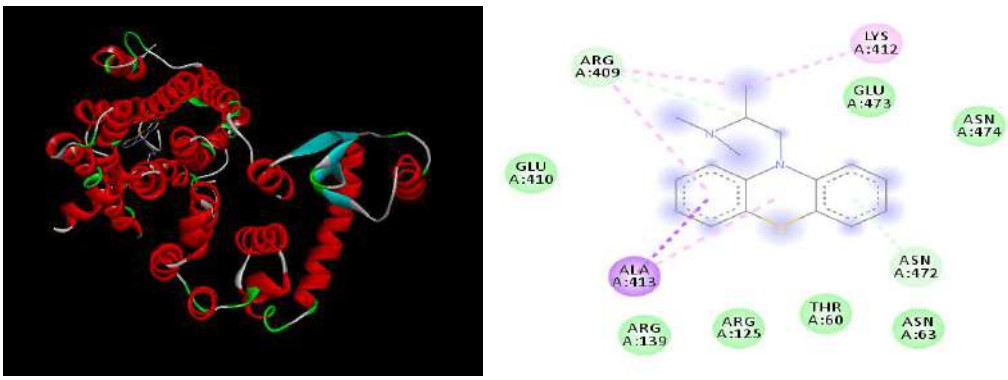

Figure 7. Interaction of Promethazine with H1 Receptor

The binding affinity of drugs present in two selected home remedies, such as lemon, and mint leaves, is also compared with the binding affinity of two commercial drugs Zofran and Granisetron on 5HT3 (serotonin receptor) and shown in Figure 8.

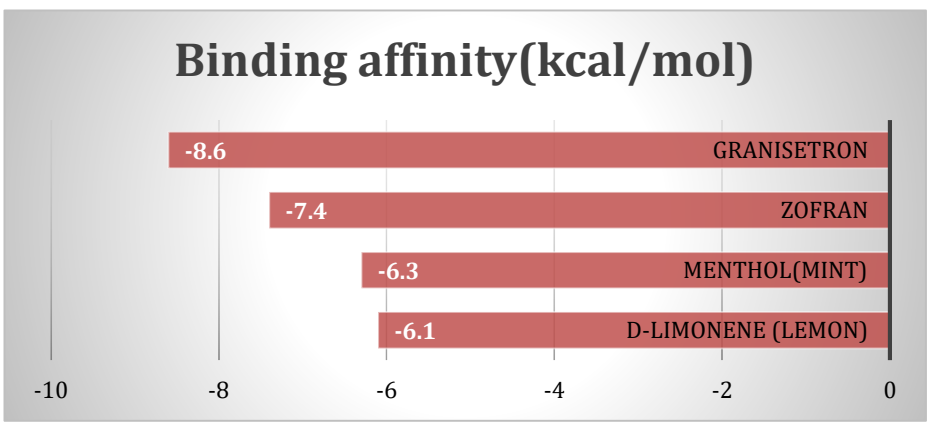

Figure 8. Binding affinity of drugs on 5HT3 receptor

Commercially available drugs such as Zofran and Granisetron have greater binding affinity values -7.4kcal/mol and -8.6 kcal/mol, respectively, on 5HT3 serotonin receptors. At the same time, home remedies, lemon, and mint have a lower binding affinity of –6.1kcal/mol and -6.3 kcal/mol, respectively. However, these values are comparatively higher than Cyclizine and Promethazine with H1 receptors.

It proves that lemon and mint have a greater binding affinity with this receptor than the H1 receptor. The interaction of the 5HT3 receptor with Lemon, Mint, Zofran, and Granisetron is shown in Figures 9,10,11,12 respectively.

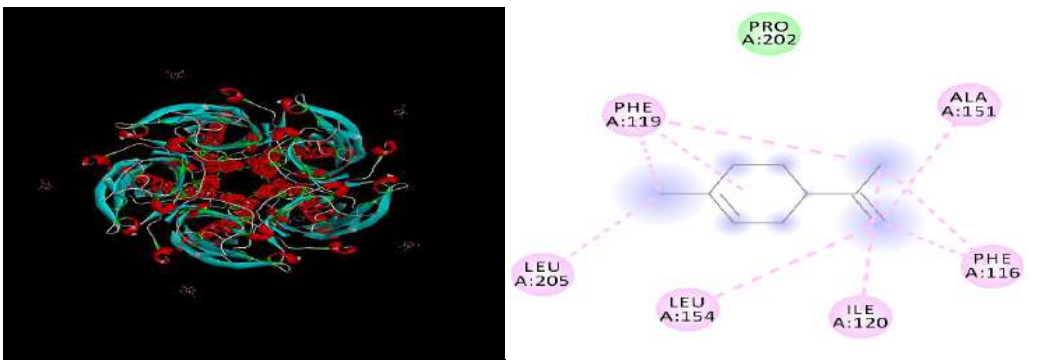

Figure 9. Interaction of D-Limonene (Lemon) with 5HT3 Receptor

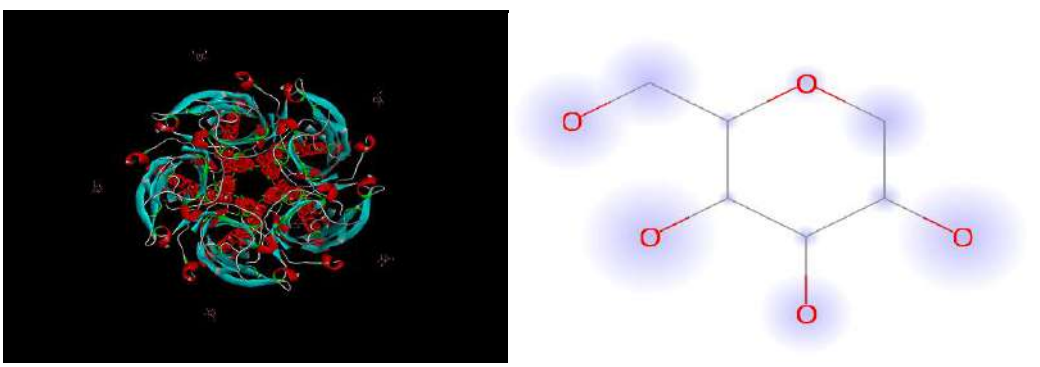

Figure 10. Interaction of Menthol (Mint) with 5HT3 Receptor

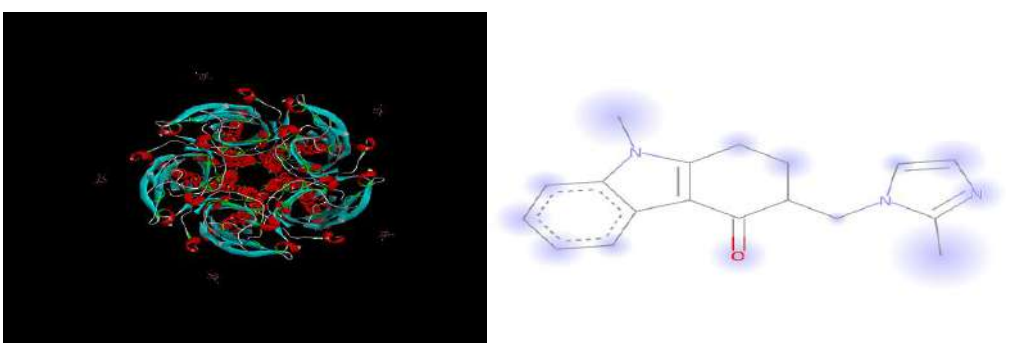

Figure 11. Interaction of Zofran with 5HT3 Receptor

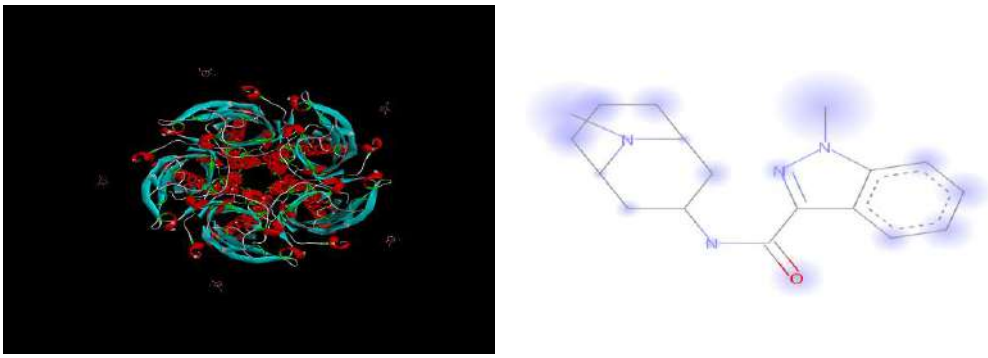

Figure 12. Interaction of Granisetron with 5HT3 Receptor

The data generated about drugs in the Swiss -ADME software is given in Table 1. It shows each drug's water solubility, absorption, etc.,

Table 1. Information about Drugs from SWISS-ADME Software

Drugs	Lipinski's Rule violations	Bioavailability Score	Water Solubility	BBB Permeance	GI absorption	Pain alert
D-Limonene (lemon)	0	0.55	soluble	yes	low	0
Ginger	2	0.17	Moderately soluble	no	low	0
Cumin oil	2	0.17	soluble	no	low	0
Menthol (mint)	0	0.55	soluble	yes	high	0
Zofran	0	0.55	Moderately soluble	yes	high	0
Granisetron	0	0.55	soluble	yes	high	0
Cyclizine	0	0.55	Moderately soluble	yes	high	0
Promethazine	0	0.55	Moderately soluble	yes	high	1

On analysing SWISS-ADME generated data results, it is seen that cumin and ginger show two violations concerning Lipinski's rule of 5 in molecular weight (should not be greater than 500 daltons) and log p-value (should be greater than 5). All other drugs show no deviation from this rule. The bioavailability score of cumin and ginger is also low, only 0.17, whereas all others have a score of 0.55. Solubility of all home remedies except ginger belongs to the class of water-soluble compounds. Granisetron is also soluble like home remedies. More excellent water solubility means excretion from the body would be much easier. All other drugs, including ginger, are moderately soluble compounds in water. Cumin and ginger do not have much Blood-Brain Barrier (BBB) permeance, whereas all others have BBB

permeance. Gastrointestinal absorption of cumin, ginger, and lemon is comparatively low, whereas all others have a high absorption rate. Natural home remedies are not causing any pain in the body, whereas, among commercial drugs, promethazine causes pain. Based on the value of binding affinity, BBB permeance, water-solubility, bioavailability score, and pain rate, the commercial drug, Granisetron is the more acceptable one for motion sickness. Home remedies are also quite good since most of it is water-soluble and offers no pain alert.

Conclusion

The commercial drugs may be fast and more effective than home remedies. From a drug point of view, our natural home remedies may have many drawbacks, but they show good binding affinity with our body's protein receptors, fewer side effects, and more water solubility. The traditional home remedies have a science behind them. Molecular docking studies like this helps in confirming it.

References

B.S. Hromatka, J.Y. Tung, A.K. Kiefer, C.B. Do, D. A. Hinds and N Eriksson (2015). Genetic variants associated with motion sickness point to roles for inner ear development, neurological processes and glucose homeostasis, *Human Molecular Genetics.* 24(9):2700-2708. doi: 10.1093/hmg/ddv028.

S. Ray (2018). Differential susceptibility of motion sickness between two phenotypically different populations of Asansol, *Research Journal of life sciences, bioinformatics, pharmaceutical, and chemical sciences*. 4(4): 516, DOI: 10.26479/2018.0404.45.

A.K.C Leung and K L Hon (2019). Motion sickness: an overview, *Drugs in Context.* 8:1-11. DOI: 10.7573/dic.2019-9-4.

A Shupak and C. R. Gordon (2006). Motion Sickness: Advances in Pathogenesis, Prediction, Prevention, and Treatment, *Aviation, Space, and Environmental Medicine.* 77(12): 1213-1223.

Koch, A., Cascorbi, I., Westhofen, M., Dafotakis, M., Klapa, S., & Kuhtz-Buschbeck, J. P. (2018). The neurophysiology and treatment of motion sickness. *Deutsches Ärzteblatt International*. 115 (41): 687. DOI: 10.3238/ arztebl.2018.0687.

MOLECULAR DOCKING STUDIES OF 3',5'-DICHOLORO-2'-HYDROXYACETOPHENONE-3-METHOXYBENZHYDRAZONE HYDRATE TOWARDS 1JXA RECEPTOR PROTEIN

Daly Kuriakose[1]* and M R Prathapachandra Kurup[2]

[1]Department of Applied Chemistry, Cochin University of Science and Technology, Kochi
[2]Department of Chemistry, St. Xavier's College for Women, Aluva
***Corresponding author email id:** dalykuriakose@gmail.com

Abstract

A tridentate ONO donor Aroylhydrazone, 3',5'-dicholoro-2'-hydroxyacetophenone-3-methoxybenzhydrazone monohydrate ($H_2CAB.H_2O$) have been synthesized and characterized by elemental analysis, LCMS, FT-IR, UV-Vis and ^1H NMR. The synthesized compound was subjected to *in vitro* antibacterial studies against a series of selected bacterial strains, by agar well diffusion method. The compound is active against *Escherichia coli.* It was further substantiated by molecular docking studies of 3',5'-dicholoro-2'-hydroxyacetophenone-3-methoxybenzhydrazone hydrate towards 1JXA receptor protein.

Keywords: Hydrazone, antibacterial, molecular docking, crystal structure

Introduction

Aroylhydrazones are well-established class of molecules with several possible structures including configurational isomers, *viz.*, *E* and *Z*, around the imine (C=N) bond and amido/iminol tautomers. Due to the presence of multiple donor sites such as protonated/deprotonated amide oxygen, imine nitrogen and additional donor site (usually N or O) provided from the carbonyl compound, they exhibit diverse chelating modes with greater effects in a wide variety of fields (Peng *et al.*, 2020; Bakir and Conry, 2016; Kuriakose *et al.*, 2017; Asha

and Kurup, 2020). The presence of the azomethine group (–NH–N=CH–) connected with carbonyl group makes them responsible for different biological activities, such as antioxidant, anti-inflammatory, anti-hypertensive, antimicrobial and anticancer properties (Nair *et al.,* 2014; Bakale *et al.,* 2014; Ebrahimipour *et al.,* 2016; Rocha, 2019; He *et al.,* 2018; Saif *et al.,* 2016). Molecular docking studies were exploited to show the possible binding mode of the test molecule with its target protein aiming to explain its antibacterial activity (Trott and Olson, 2010; Dallakyan and Olson, 2015; Morris *et al.,* 1998). The present study reports the molecular docking studies of 3',5'-dicholoro-2'-hydroxyacetophenone-3-methoxybenzhydrazone hydrate towards 1JXA receptor protein.

Materials and Methods

The chemicals and solvents used in the syntheses were used without further purification. The chemicals, 3′,5′-dichloro-2′-hydroxyacetophenone (Aldrich), 3-methoxybenzhydrazide (Alfa Aesar) used were of analar quality. Methanol was purchased from Spectrochem. The aroylhydrazone ($H_2CAB·H_2O$) was synthesized by a previously reported procedure (Kuriakose and Kurup, 2020).

Synthesis details

Synthesis of 3′,5′-dichloro-2′-hydroxyacetophenone-3-methoxybenzoylhydrazone monohydrate ($H_2CAB·H_2O$). 3-Methoxybenzhydrazide (0.17 g, 1.00 mmol) dissolved in 10 mL methanol, 3′,5′-dichloro-2′-hydroxyacetophenone (0.21 g, 1.00 mmol) dissolved in 10 mL methanol was added and refluxed for 4 h. Single crystals suitable for X-ray analysis obtained on evaporation of the resulting reaction mixture were separated, washed and dried over P_4O_{10} in vacuo (Kuriakose and Kurup, 2020) (Scheme 1).

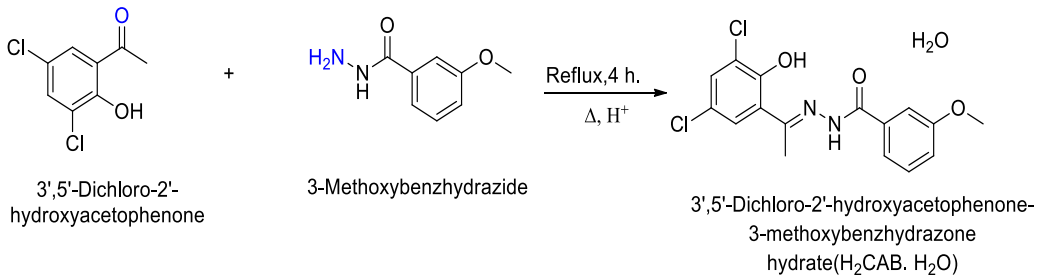

3',5'-Dichloro-2'-hydroxyacetophenone

3-Methoxybenzhydrazide

3',5'-Dichloro-2'-hydroxyacetophenone-3-methoxybenzhydrazone hydrate(H_2CAB. H_2O)

Scheme 1. Synthesis of $H_2CAB \cdot H_2O$.

Analytical data for $C_{16}H_{16}Cl_2N_2O_4$ ($H_2CAB \cdot H_2O$) Yield: 0.29 g (77%); color: Yellow; M.W.: 371.21 g mol^{-1}; elemental analysis calculated/found (%): C 51.8/51.7, H 4.3/4.5, N 7.6/7.8; ^{1}H NMR (400 MHz, DMSO-*d*6): δ 2.86 (3H, *s*, $–CH_3$), 3.85 (3H, *s*, $–OCH_3$), 7.22 (1H, *q*, aromatic), 7.5 (3H, *m*, aromatic), 7.63 (1H, *d*, aromatic), 7.68 (1H, *d*, aromatic), 11.55 (1H, *br*, OH), 14.43 (1H, *br*, NH); FT–IR: ν (cm^{-1}) 3548 ν(O–H), 3439 ν(N–H), 1660 ν(C=O), 1592, ν(C=N). MS (ESI) m/z (M+1) 353.1, calculated m/z 352.04.

Physical measurements

The micro-analyses of carbon, hydrogen and nitrogen were performed on a Vario EL III CHNS analyzer. IR spectra of the compounds were recorded in KBr pellets with FTIR spectrometer (JASCO-4100) in the region 4000–400 cm^{-1}. The proton NMR spectra were collected in DMSO-d_6 on a Bruker Avance III, 400 MHz spectrometer having 9.4 T superconducting magnet using tetramethylsilane (TMS) as an internal reference. Electronic spectra in DMF solutions were recorded on a Thermo scientific evolution 201 UV–Vis double beam spectrophotometer in the 200–800 nm range. The LCMS analysis of the aroylhydrazone was performed using Waters e265 mass detector.

Antibacterial studies

The aroylhydrazone, $H_2CAB.H_2O$ was screened against one Gram positive (*Bacillus subtilis*) and two Gram negative (*Escherichia coli* and *Klebsiella pneumoniae*) human pathogenic bacteria. Antibacterial activity was assessed by using Agar well diffusion method (Perez, 1990; Ganji *et al.,* 2018). The test solutions were prepared by dissolving 1000 mg of test sample in 1 mL of N, N-dimethyl sulfoxide (DMSO). Ampicillin was used as positive control. The bacteria were grown in nutrient agar medium and incubated at 37 °C for 48 h to obtain the primary culture. Each bacterial culture was swabbed on to labeled Muller Hinton Agar plate with the help of sterile swab. Wells (8 mm diameter) were made into the agar medium and that was prepared with the back of sterile micro tip. The wells in the Petri plates were loaded with 200 mL of each of the test compound. Then the plates were incubated 24-h at 37 °C. Microbial growth was determined by measuring the diameter (well diameter included) of the zone of inhibition. All tests were done in triplicate.

Results and discussion

Facile condensation of 3′,5′-dichloro-2′-hydroxyacetophenone with 3-methoxybenzhydrazide in 1:1 ratio led to the formation of 3′,5′-dichloro-2′ -hydroxyacetophenone-3-methoxybenzoylhydrazone monohydrate.

The aroylhydrazone and the complex obtained are stable towards air and moisture in the solid state at room temperature. The partial elemental analyses for the hydrazone are in good agreement with the given molecular formulae, which confirm the analytically pure nature of the samples. The aroylhydrazone was characterized using various physicochemical techniques (Figure 1).

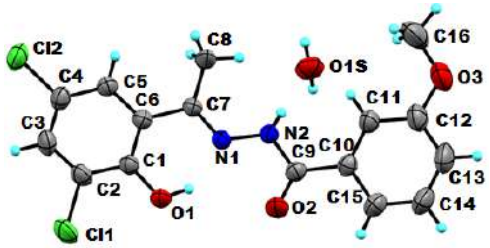

Figure 1. ***ORTEP*** **diagram of $H_2CAB.H_2O$ depicting molecular structure along with atom labelling scheme for all non-hydrogen atoms. Displacement ellipsoids are drawn at 30% probability**

Antibacterial activity

The bacteria selected for present investigations included –*Bacillus subtilis*, *Escherichia coli* and *Klebsiella pneumoniae*. The results showed that both the compound displayed bactericidal activity against against all the selected test organisms. A possible explanation is that Gram negative bacteria have lipopolysaccharide (LPS) layer on the outer surface. This major component is an important entity in determining the outer membrane barrier function of Gram negative bacteria. The aroylhydrazone can penetrate the bacterial cell membrane and leads to the damage of outer cell membrane (Table 1).

Table 1. Antibacterial activities of $H_2CAB.H_2O$.

Compound	**Diameter of zone of inhibition (mm)**		
	Gram positive	**Gram positive**	
$H_2CAB.H_2O$	*B. subtilis* 2	*E. coli* 9	*K. pneumonia* 3

Molecular docking

The AutoDock is an automatic docking programme designed for the prediction of the binding among small molecules for- example drug candidates and the receptor having known 3D structure (Hassan *et al.*, 2018; Tan *et al.*, 2020; Bansode *et al;* 2019; Tahlan *et al.*, 2019; Luo *et al.*, 2019; Zhang *et al.*, 2019; Shah *et al.*, 2020). Molecular docking studies were performed using AutoDock 4.2 Vina software to confirm the antibacterial activity 3′,5′-dichloro-2′-hydroxyacetophenone

-3-methoxybenzoylhydrazone monohydrate against proteins *viz* 1JXA. Crystal structure of the target proteins were downloaded from the RSCB PDB website in the PDB format (Berman *et al.*, 2000). Before docking, the water molecules and other co-crystallized ligand molecules were removed from the target proteins and polar hydrogens were added using PyMoL software (Schrodinger, 2020). The active site of the protein was explained within the grid size 30 ˚A ×30 ˚A ×30 ˚A in order to incorporate the residues of the active sites. The best fit conformation was analysed, which is based on the binding score, hydrogen bonding and other hydrophobic interactions. The binding interactions were visualized using Discovery studio visualizer. Affinity of best docked position of the molecule and protein target complex was determined by E-value (kcal/mol). It provides the prediction of binding free energy for docked molecule (Ganji *et al.*, 2018). The target protein IJXA shows a good binding affinity (E) -9.1 k cal/mol^{-1}. So, we can use it as the best antibacterial drugs (Figure 2).

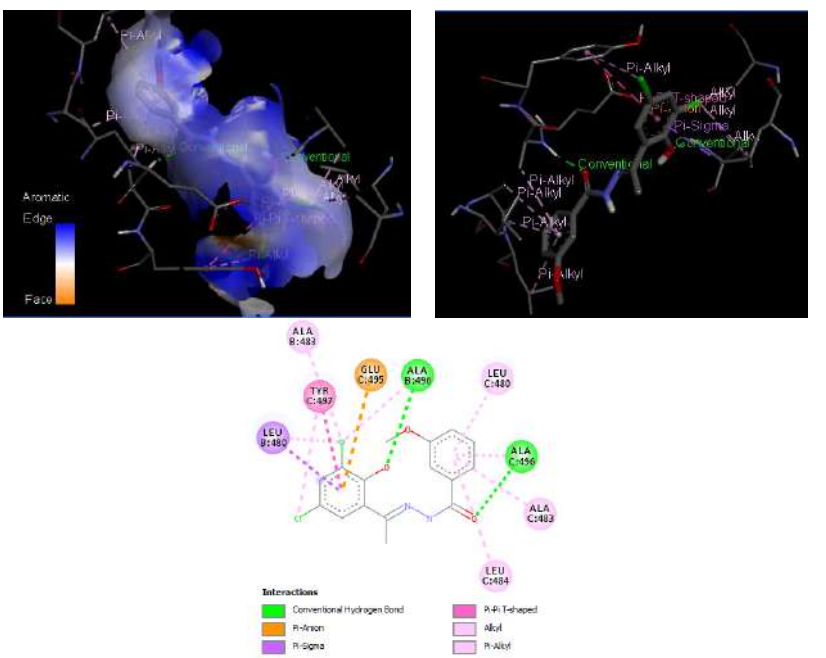

Figure 2. 3D & 2D diagram $H_2CAB.H_2O$ docked into the binding site of anti-bacterial proteins.

Conclusion

The present paper deals with the synthesis of ONO donor aroylhydrazone $H_2CAB.H_2O$. The compound was subjected to antibacterial studies against *Bacillus subtilis, Escherichia coli* and *Klebsiella pneumoniae*. The compound is more active against *Escherichia coli* which was further substantiated by molecular docking studies.

Acknowledgement

Daly Kuriakose thanks the University Grants Commission, New Delhi, India for the award of a Senior Research Fellowship (F.17-45/2008(SA-1) dated 11.08.2014). The authors are also thankful to the Sophisticated Analytical Instrumentation Facility, Cochin University of Science and Technology, Kochi, India for elemental analyses, 1H-NMR and single crystal X-ray diffraction measurements. Dr. Sylas V. P., Department of Environmental Science, Mahatma Gandhi University, Kottayam, India is acknowledged for antibacterial studies.

References

Asha, T. M. and Kurup, M. R. P. (2020) Synthesis, structural insights and catalytic activity of a dioxidomolybdenum (VI) complex chelated with N4-(3-methoxyphenyl) thiosemicarbazone. *Transition Metal Chemistry*. 45(7): 467-476.

Bakale, R. P., Naik, G. N., Mangannavar, C. V., Muchchandi, I. S., Shcherbakov, I. N., Frampton, C. and Gudasi, K. B. (2014) Mixed ligand complex via zinc (II)-mediated in situ oxidative heterocyclization of hydrochloride salt of 2-chlorobenzaldehyde hydralazine hydrazone as potential of antihypertensive agent. *European Journal of Medicinal Chemistry*. 73: 38-45.

Bakir, M. and Conry, R. (2016) Synthesis, spectroscopic and X-ray crystallographic properties of manganese compounds of keto-and enol-coordinated di-2-pyridyl ketone benzoyl hydrazone (dpkbh). Reactions of [Mn (CO) 5Br] with dpkbh. *Journal of Coordination Chemistry*. 69 (7): 1244-1257.

Bansode, P., Patil, P., Choudhari, P., Bhatia, M., Birajdar, A., Somasundaram, I. and Rashinkar, G. (2019) Anticancer activity and molecular docking studies of ferrocene tethered ionic liquids. *Journal of Molecular Liquids.* 290: 111182.

Berman, H. M., Westbrook, J., Feng, Z., Gilliland, G., Bhat, T. N., Weissig, H., ... and Bourne, P. E. (2000) The protein data bank. *Nucleic acids research*. 28 (1): 235-242.

Dallakyan, S. and Olson, A. J. (2015) Small-molecule library screening by docking with PyRx. In *Chemical biology* (pp. 243-250). Humana Press, New York, NY.

Ebrahimipour, S. Y., Sheikhshoaie, I., Simpson, J., Ebrahimnejad, H., Dusek, M., Kharazmi, N. and Eigner, V. (2016) Antimicrobial activity of aroylhydrazone -based oxido vanadium (v) complexes: In vitro and in silico studies. *New Journal of Chemistry*. 40 (3): 2401-2412.

Ganji, N., Rambabu, A., Vamsikrishna, N. and Daravath, S. (2018) Copper (II) complexes with isoxazole Schiff bases: Synthesis, spectroscopic investigation, DNA binding and nuclease activities, antioxidant and antimicrobial studies. *Journal of Molecular Structure.* 1173*:* 173-182.

Hassan, M., Ashraf, Z., Abbas, Q., Raza, H. and Seo, S. Y. (2018) Exploration of novel human tyrosinase inhibitors by molecular modeling, docking and simulation studies. *Interdisciplinary sciences: computational life sciences.* 10 (1): 68-80.

He, L. Y., Qiu, X. Y., Cheng, J. Y., Liu, S. J. and Wu, S. M. (2018) Synthesis, characterization and crystal structures of vanadium (V) complexes derived from halido-substituted tridentate hydrazone compounds with antimicrobial activity. *Polyhedron*. 156: 105-110.

Kuriakose, D. and Kurup, M. P. (2020) Synthesis, spectral, structural and antibacterial studies of ONO donor aroylhydrazone and its Mo (VI) complex. *Journal of Molecular Structure*. 1213*:* 128188.

Kuriakose, D., Aravindakshan, A. A. and Kurup, M. P. (2017) Synthesis, spectroscopic, crystal structures and photoluminescence studies of cadmium (II) complexes derived from di-2-pyridyl ketone benzoylhydrazone: Crystal structure of a rare eight coordinate cadmium (II) complex. *Polyhedron*. 127: 84-96.

Luo, Z., Valeru, A., Penjarla, S., Liu, B. and Khan, I. (2019) Synthesis, anticancer activity and molecular docking studies of novel pyrido [1, 2-a] pyrimidin-4-one derivatives. *Synthetic Communications*. 49 (17): 2235-2243.

Morris, G. M., Goodsell, D. S., Halliday, R. S., Huey, R., Hart, W. E., Belew, R. K. and Olson, A. J. (1998) Automated docking using a Lamarckian genetic algorithm and an empirical binding free energy function. *Journal of computational chemistry*. 19 (14): 1639-1662.

Nair, R. S., Kuriakose, M., Somasundaram, V., Shenoi, V., Kurup, M. P. and Srinivas, P. (2014) The molecular response of vanadium complexes of nicotinoyl hydrazone in cervical cancers—a possible interference with HPV oncogenic markers. *Life sciences*. 116 (2): 90-97.

Peng, H., Peng, X., Huang, J., Huang, A., Xu, S., Zhou, J., ... and Cai, X. (2020) Synthesis and crystal structure of a novel pyridine acylhydrazone derivative as a "turn on" fluorescent probe for Al3+. *Journal of Molecular Structure.* 1212: 128138.

Perez, C. (1990) Antibiotic assay by agar-well diffusion method. *Acta Biol Med Exp*. 15: 113-115.

Rocha, C. S. (2019) LFOB Filho, AE De Souza, R. Diniz, AML Denadai, H. Beraldo, LR Teixeira. *Polyhedron*. 170: 723-730.

Saif, M., El-Shafiy, H. F., Mashaly, M. M., Eid, M. F., Nabeel, A. I. and Fouad, R. (2016) Synthesis, characterization, and antioxidant/cytotoxic activity of new chromone Schiff base nano-complexes of Zn (II), Cu (II), Ni (II) and Co (II). *Journal of Molecular Structure*. 1118: 75-82.

Schrodinger, L. L. C. (2010) The PyMOL molecular graphics system. *Version*. 1(5): 0.

Shah, S. R., Katariya, K. D. and Reddy, D. (2020) Quinoline-1, 3-Oxazole hybrids: syntheses, anticancer activity and molecular docking studies. *Chemistry Select*. *5*(3): 1097-1102.

Tahlan, S., Narasimhan, B., Lim, S. M., Ramasamy, K., Mani, V. and Shah, S. A. (2019) 2-Mercaptobenzimidazole Schiff bases: design, synthesis, antimicrobial studies and anticancer activity on HCT-116 cell line. *Mini reviews in medicinal chemistry*. 19 (13): 1080-1092.

Tan, A., Kizilkaya, S., Kelestemur, U., Akdemir, A. and Kara, Y. (2020) The synthesis, anticancer activity, structure-activity relationships and molecular modelling studies of novel isoindole-1, 3 (2H)-dione compounds containing different functional groups. *Anti-Cancer Agents in Medicinal Chemistry (Formerly Current Medicinal Chemistry-Anti-Cancer Agents)*. 20 (11): 1368-1378.

Trott, O. and Olson, A. J. (2010) AutoDock Vina: improving the speed and accuracy of docking with a new scoring function, efficient optimization, and multithreading. *Journal of computational chemistry*. 31(2): 455-461.

Zhang, Y. L., Yang, R., Xia, L. Y., Man, R. J., Chu, Y. C., Jiang, A. Q., ... and Zhu, H. L. (2019) Synthesis, anticancer activity and molecular docking studies on 1, 2-diarylbenzimidazole analogues as anti-tubulin agents. *Bioorganic Chemistry*. 92: 103219.

INSTRUCTIONS TO AUTHORS

Research Articles (not exceeding 4000 words) should be the results of original, unpublished research work in various academic disciplines.

Review articles (not exceeding 4000 words) are expected to survey and discuss current developments in a field.

Short Communication (not exceeding 2000 words) are brief accounts on projects undertaken. They should include a brief abstract and an introductory paragraph

Manuscript Preparation

The manuscript should be ordered as follows: Title page, abstract, key words, text, acknowledgements, references, figure and table legends, figures and tables. All manuscripts should be typeset in MS Word (Font: Times New Roman; Size: 12 points) double-spaced with at least 1" margin from all sides. Manuscript pages should be serially numbered.

Title Page*:* The first page of the article should contain the title of the paper, the names of authors, affiliations and addresses. The address of the corresponding author should be provided in full.

Abstract: The second page must contain an abstract of not more than 200 words and 3-5 keywords.

Text*:* The text of an article should be divided into Introduction, Materials and Methods, Results, Discussion and Conclusion.

Tables and Figures: All figures and tables should be included as separate sheets or files, are to be numbered using Arabic numerals and be cited in text in consecutive numerical order. Figures should be uploaded separately, not embedded in the article file. Soft copies of figures in Tagged Image Format or Joint Photographic Experts Group (TIFF or JPEG) with at least 300 dpi resolution in Grayscale mode is preferred. Use the table function, not spread sheets, to make tables. Legends to tables and figures may be provided on a separate page.

Abbreviations, Characters and Units: Define abbreviations that are not standard ina footnote to be placed on the first page of the article. Superscripts, subscripts and ambiguous characters should be clearly indicated. Units of measure should be metric or, preferably, SI.

Acknowledgements: The acknowledgements of people, grants, funds, etc. should be given at the end of the paper, before the reference list and should be as brief as possible. The names of funding organizations should be written in full.

References: The list of references should only include works that are cited in the text and that have been published or accepted for publication. Personal communications and unpublished works should only be mentioned in the text. Reference list entries should be alphabetized by the last names of the first author of each work.

Journal article

Amann RI, Ludwig W, Schleifer K-H (1995) Phylogenetic identification and *in situ* detection of individual microbial cells without cultivation. Microbiological Reviews 59: 143 – 165

Book

Bull AT (2004) Microbial diversity and bioprospecting. ASM press, New York

Online document

Cartwright J (2007) Big stars have weather too. IOP Publishing PhysicsWeb.http:// physicsweb.org/articles/news/11/6/16/1. Accessed 26 June 2007

SUBSCRIPTION/ RENEWAL ORDER FORM

I/We would like to subscribe/ renew the journal for ----- years.

Mailing address: (BLOCK CAPITALS ONLY)

Name:.....

Address: .....

.....

.....

City.....State.....PIN ..... .

Telephone:.....email:.....

I /We enclose a DD/Cheque

No.....dated..... .....

drawn on .....(Bank) for.....rupees

Signature .....

DECLARATION

FORM I (See Rule- 3)

STATEMENT ABOUT OWNERSHIP AND OTHER PARTICULARS OF THE JOURNAL

1.	Title of the Publication	Discourse
2.	Place of Publication	Aluva
3.	Periodicity of the Publication	Biannual
4.	Printer's Name	Dr. Sr. Geege Joanamma Xavier (Principal)
	(Whether citizen of India?	Yes, Indian
	If foreign, state the country of origin)	
	Address	St. Xavier's College for Women, Aluva, Ernakulam
5.	Publisher's Name	Dr. Sr. Geege Joanamma Xavier (Principal)
	(Whether citizen of India?	
	If foreign, state the country of origin)	Yes, Indian
	Address	St. Xavier's College for Women, Aluva, Ernakulam
6.	Chief Editor's Name	Dr. Anu Anto
	(Whether citizen of India?)	Yes
		Assistant Professor, Department of Zoology, St. Xavier's College for Women, Aluva, Ernakulam
7.	Name and address of individuals who own the newspaper and partners and shareholders holding more than one percent of the total capital	St. Xavier's College for Women, Aluva Ernakulam Kerala

I, Dr. Anu Anto, hereby declare the particulars given above are true to the best of my knowledge.

Aluva,
01-03-2022

(Sd/-)
Dr. Anu Anto

Vol. 10 No.1 March 2022 ISSN 2321-0214

Printed and published by Principal St.Xavier's College Aluva, Ernakulam Dist.
Printed at. Indu Photos Kalamassery